Cancer Cell
Article

The RhoGEF GEF-H1 Is Required for Oncogenic RAS Signaling via KSR-1

Jane Cullis,[1,3,10] David Meiri,[1,10] Maria Jose Sandi,[1] Nikolina Radulovich,[1,5] Oliver A. Kent,[1] Mauricio Medrano,[1,3] Daphna Mokady,[1] Josee Normand,[1] Jose Larose,[1] Richard Marcotte,[1] Christopher B. Marshall,[1] Mitsuhiko Ikura,[1,3] Troy Ketela,[6,8] Jason Moffat,[6,8] Benjamin G. Neel,[1,3,5] Anne-Claude Gingras,[6,9] Ming-Sound Tsao,[1,3] and Robert Rottapel[1,2,3,4,7,*]

[1]Princess Margaret Cancer Center, University Health Network, 101 College Street, Room 8-703, Toronto Medical Discovery Tower, University of Toronto, Toronto, ON M5G 1L7, Canada
[2]Department of Medicine, University of Toronto, 1 King's College Circle, Toronto, ON M5S 1A8, Canada
[3]Department of Medical Biophysics, University of Toronto, 1 King's College Circle, Toronto, ON M5S 1A8, Canada
[4]Department of Immunology, University of Toronto, 1 King's College Circle, Toronto, ON M5S 1A8, Canada
[5]Department of Laboratory Medicine and Pathobiology, University of Toronto, 1 King's College Circle, Toronto, ON M5S 1A8, Canada
[6]Department of Molecular Genetics, University of Toronto, 1 King's College Circle, Toronto, ON M5S 1A8, Canada
[7]Division of Rheumatology, St. Michael's Hospital, 30 Bond Street, Toronto, ON M5B 1W8, Canada
[8]Donnelly Centre and Banting and Best Department of Medical Research, 160 College Street, Room 8-804, University of Toronto, Toronto, ON M5S 3E1, Canada
[9]Lunenfeld-Tanenbaum Research Institute, Mount Sinai Hospital, 600 University Avenue, Room 992A, Toronto, ON M5G 1X5, Canada
[10]These authors contributed equally to this work
*Correspondence: rottapel@uhnresearch.ca
http://dx.doi.org/10.1016/j.ccr.2014.01.025

SUMMARY

Cellular transformation by oncogenic RAS engages the MAPK pathway under strict regulation by the scaffold protein KSR-1. Here, we report that the guanine nucleotide exchange factor GEF-H1 plays a critical role in a positive feedback loop for the RAS/MAPK pathway independent of its RhoGEF activity. GEF-H1 acts as an adaptor protein linking the PP2A B' subunits to KSR-1, thereby mediating the dephosphorylation of KSR-1 S392 and activation of MAPK signaling. GEF-H1 is important for the growth and survival of $HRAS^{V12}$-transformed cells and pancreatic tumor xenografts. GEF-H1 expression is induced by oncogenic RAS and is correlated with pancreatic neoplastic progression. Our results, therefore, identify GEF-H1 as an amplifier of MAPK signaling and provide mechanistic insight into the progression of RAS mutant tumors.

INTRODUCTION

The centrality of the RAS/MAPK pathway in promoting tumor formation is underscored by the high frequency of gain-of-function mutations in RAS family members and other components of the pathway in human cancers. KRAS has a particularly high mutation frequency of 30%–50% in colon and greater than 90% in pancreatic adenocarcinomas (Oliveira et al., 2007; Mulcahy et al., 1998). The importance of RAS is a reflection of its essential role in mediating the transduction of signals from growth factor receptors to pathways that regulate transcription, cell cycle progression, cell shape, and cell survival, all of which are commonly disturbed in cancer (Macara et al., 1996). RAS engages diverse signaling pathways, including RAF, PI3K, RAL-GDS, and TIAM-1, each of which are also subject to activating mutations in cancer (Davies et al., 2002; Samuels and Velculescu, 2004; Philp et al., 2001; Sjöblom et al., 2006; Greenman et al., 2007; Engers et al., 2000). RAS activation is coupled to transcription through the activation of the MAPK cascade, involving the sequential phosphorylation and activation of the serine/threonine kinases RAF (MAPKKK), MEK1/2 (MAPKK), and ERK1/2 (MAPK)

Significance

Mutational activation of RAS occurs in over 90% of pancreatic cancers and is required for both the initiation and progression of tumorigenesis. However, the mechanism of RAS-mediated cellular transformation is not fully understood. Here, we find that GEF-H1 is necessary for optimal RAS/MAPK pathway signaling and contributes to the growth and survival of RAS mutant cells. GEF-H1 expression is induced by oncogenic RAS and is elevated in pancreatic tumor samples, thereby providing an amplifying loop for RAS/MAPK signaling. Our results, therefore, extend our understanding of the signaling dependencies of oncogenic RAS, which may ultimately improve the development of RAS-pathway-directed therapeutics.

(Moodie et al., 1993; Warne et al., 1993; Zhang et al., 1993; Vojtek et al., 1993).

The Kinase Suppressor of RAS (KSR-1) was originally identified in genetic screens in *Drosophila* and *Caenorhabditis elegans* designed to isolate mutations in genes that modify the phenotypes associated with oncogenic RAS alleles (Jacobs et al., 1999; Therrien et al., 1995; Sundaram and Han, 1995). In mammalian cells, KSR-1 acts as a molecular scaffold to assemble a macromolecular complex of MAPK pathway components to facilitate efficient signal transmission (Therrien et al., 1996; Michaud et al., 1997; Cacace et al., 1999; Morrison, 2001) and is required for mutant RAS-mediated cellular transformation (Nguyen et al., 2002; Lozano et al., 2003). KSR-1 also functions as a gate to control flux through the MAPK pathway. In quiescent cells, KSR-1 is phosphorylated on S297 and S392 by C-TAK1 and held in an inactive state in the cytosol by 14-3-3 proteins (Ory et al., 2003). RAS activation stimulates the dephosphorylation of KSR-1 on S392, resulting in its translocation to the plasma membrane where it potentiates MAPK signaling (Ory et al., 2003).

Genetic studies performed in model organisms showed that mutations in the PP2A phosphatase phenocopied a loss of KSR-1 function in a RAS mutant background (Wassarman et al., 1996; Sieburth et al., 1999), suggesting that PP2A is a positive regulator of KSR-1. PP2A was subsequently shown to be the critical phosphatase required for dephosphorylation of KSR-1 on S392 in response to activated RAS (Ory et al., 2003). PP2A is a heterotrimeric serine/threonine protein phosphatase composed of a catalytic (C), structural (A), and regulatory (B) subunit. The catalytic and structural subunits are constitutively associated to form a core complex to which one of many B subunits can bind (Janssens and Goris, 2001). Four different B subunits (B, B', B'', and B''') exist in mammals that determine the localization and substrate specificity of the holoenzyme (Janssens and Goris, 2001). The A and C subunits constitutively associate with KSR-1, whereas association of the B' subunit is induced only upon RAS activation (Ory et al., 2003). The mechanism by which the B' subunit is recruited to KSR-1 has yet to be elucidated.

GEF-H1, which is encoded by *ARHGEF2*, is a microtubule-associated guanine nucleotide exchange factor (GEF) for the Rho family of small GTPases (Ren et al., 1998). Several lines of evidence have highlighted the transforming potential of GEF-H1. *ARHGEF2* is amplified in hepatocellular carcinoma (Cheng et al., 2012) and is a transcriptional target of gain-of-function p53 mutants (Mizuarai et al., 2006) and the metastasis-associated hPTTG1 (Liao et al., 2012). Truncated versions of GEF-H1 can transform NIH 3T3 cells (Whitehead et al., 1995) and induce tumor formation in nude mice (Brecht et al., 2005). *ARHGEF2* is one of six genes significantly downregulated in response to imatinib treatment in gastrointestinal tumors (Frolov et al., 2003). In addition, *ARHGEF2* was identified in a genome-wide pooled small hairpin RNA (shRNA) screen designed to identify genes that are required for the survival of human breast, colon, lung, ovarian, and pancreatic cell lines (Marcotte et al., 2012). These data suggest that GEF-H1 may be a marker for and/or contribute to tumorigenesis in multiple contexts.

RESULTS

GEF-H1 Contributes to the Survival of a Subset of Human Cancer Cell Lines, and Its expression Is Regulated by the RAS/MAPK Pathway

GEF-H1 was found to contribute to the competitive growth characteristics of 18 out of 73 cell lines, 13 of which were identified in the original shRNA screen and 5 of which were identified in our secondary screen (Figure 1A and Table S1 available online). For further validation, we selected three of these cell lines and stably infected them with two distinct lentiviral hairpins directed against GEF-H1. Cells depleted of GEF-H1 exhibited decreased growth and increased death relative to control hairpin-expressing cells as assessed by caspase 3 cleavage (Figures 1B and S1A–S1H). These data suggest that GEF-H1 is important for cell growth and survival in several human cell lines derived from different tumor types.

We noted that GEF-H1 dependency was enriched in RAS/BRAF mutant cell lines (13 of 30 [43.3%]) compared to RAS/BRAF wild-type cell lines (5 of 43 [11.6%]). GEF-H1 was found to contribute to cell growth/survival in 10 of 25 (40%) KRAS mutant pancreatic cancer cell lines with little effect on the three wild-type KRAS pancreatic cancer cell lines (Table S1). We therefore explored the possibility that GEF-H1 sensitivity in some cellular contexts is epistatic with gain-of-function mutations in the RAS/MAPK pathway. Because elevated expression of GEF-H1 is transforming in NIH 3T3 cells (Whitehead et al., 1995), we examined the ability of mutant RAS family members to induce GEF-H1 expression in a common isogenic cellular background. We observed that GEF-H1 protein levels were increased in cells transformed by each mutant RAS family member compared to nontransformed cells (Figure 1C). We next determined whether the induction of GEF-H1 expression was a direct result of activated RAS or a secondary consequence of the transformed state. We used a murine embryonic fibroblast (MEF) cell line expressing a hydroxytamoxifen (4-OHT)-inducible form of $HRAS^{V12}$ (ER:$HRAS^{V12}$) (Gupta et al., 2007) and found that GEF-H1 expression increased within 15 min of ER:$HRAS^{V12}$ induction and continued to increase with progressive elevation of ER:$HRAS^{V12}$ expression (Figure 1D, upper panel). Cells treated with vehicle control (EtOH) exhibited no change in GEF-H1 levels (Figure 1D, lower panel). These data show that GEF-H1 is induced acutely in response to expression of $HRAS^{V12}$. MAP kinase pathway activation followed a bimodal distribution, peaking at 15 min and 8 hr after $HRAS^{V12}$ induction, but decreasing over intermediate time points, as has been previously shown (Gupta et al., 2007).

ARHGEF2 Is a Transcriptional Target of the RAS/MAPK Pathway

To assess whether GEF-H1 expression was dependent on MAPK activation, we treated OV-90, HCT116, and Panc 02.03 cells with the MEK1/2 inhibitors PD98059 and UO126 and found that the GEF-H1 protein level decreased following MEK1/2 inhibition (Figure 2A). Similar findings were observed in $HRAS^{V12}$-transformed NIH 3T3 cells (Figure 2B). We noted that the GEF-H1 mRNA level was elevated 2-fold in $HRAS^{V12}$-transformed NIH 3T3 cells relative to wild-type cells (Figure 2C) and sought to determine whether *ARHGEF2* was a direct

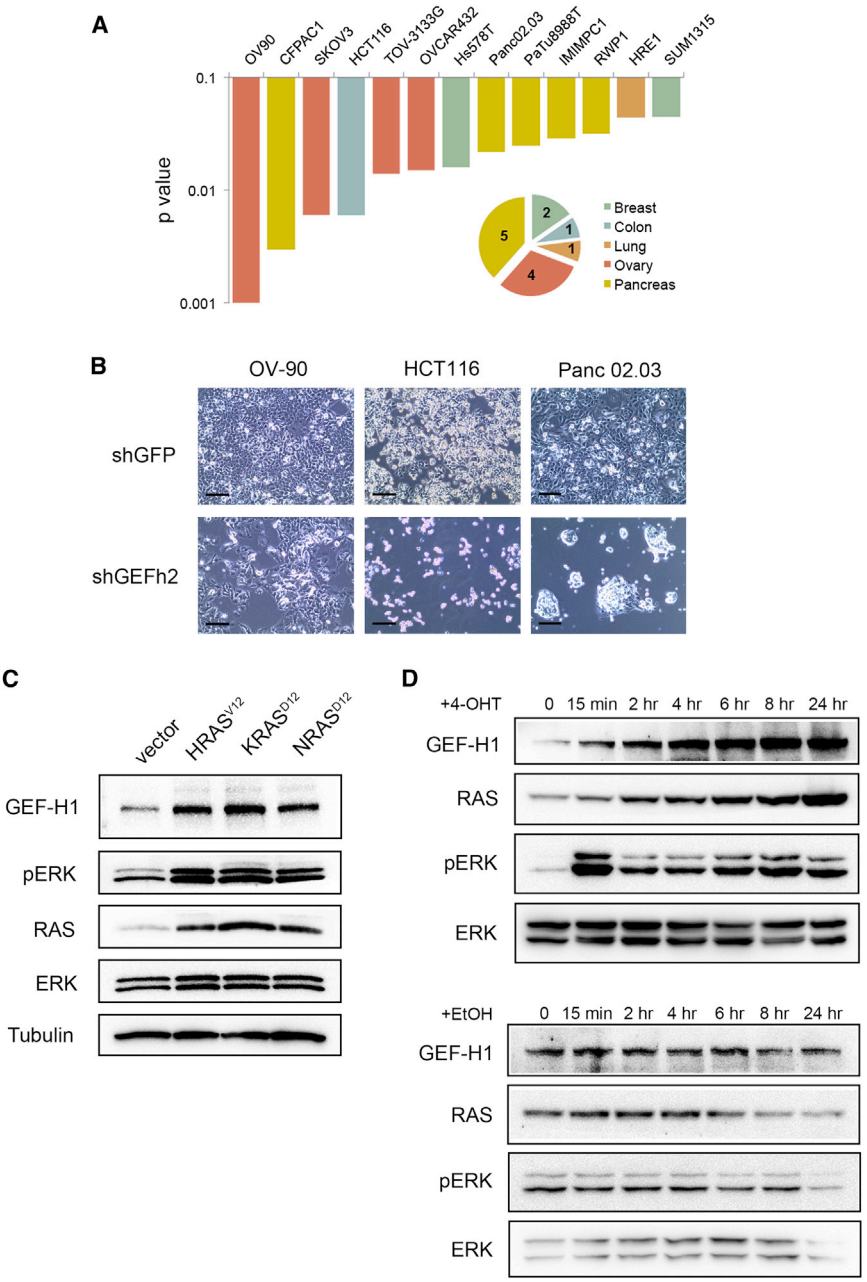

Figure 1. GEF-H1 Contributes to the Survival Fitness of a Subset of Human Cancer Cell Lines, and Its Protein Expression Is Regulated by the RAS/MAPK Pathway

(A) Schematic graphical representation of 13 GEF-H1-sensitive cell lines arranged according to the p values for the normalized Genetic Activity Rank Profile (zGARP) score across 75 cell lines (Marcotte et al., 2012). The fraction of GEF-H1-sensitive cell lines from each tumor type is depicted by the pie chart. The number of cell lines showing GEF-H1 dependency is indicated within the area of each slice.

(B) Bright field images of the indicated cells 6 days following infection and selection with hairpin control (shGFP) or human GEF-H1 shRNA (shGEFh2) lentivirus. Scale bars, 100 μm.

(C) Immunoblot analysis of GEF-H1 and RAS expression in NIH 3T3 cells stably expressing vector, T7-HRAS^{V12}, T7-KRAS^{D12}, or T7-NRAS^{D12}. pERK indicates level of MAPK pathway activation and total ERK and tubulin served as protein loading controls.

(D) Immunoblot analysis of GEF-H1 expression following acute induction of ER:HRAS^{V12} with 100 nM 4-OHT (upper panel) or treatment with vehicle control (lower panel) over the indicated period of time.

See also Figure S1 and Table S1.

transcriptional target of mutant RAS. Based on phylogenetic footprinting and CpG island enrichment, we identified a 1.9 kb region upstream of the first exon of murine *Arhgef2* predicted to contain the putative promoter, and we cloned this region into a luciferase reporter (Figure 2D). Expression of HRAS^{V12} induced a 7-fold increase in the normalized *Arhgef2* promoter-mediated luciferase activity compared to NIH 3T3 cells expressing the *Arhgef2* promoter alone and was quenched following MEK inhibition (Figure 2E). Together, these data show that *Arhgef2* is a transcriptional target of the RAS/MAPK pathway and that the elevated GEF-H1 protein level observed in HRAS^{V12}-transformed cells are, at least in part, due to elevated transcription.

GEF-H1 Contributes to Cell Survival and Growth in HRAS^{V12}-Transformed Cells

We next sought to determine whether GEF-H1 was important for HRAS^{V12}-mediated cellular transformation. We stably knocked down murine GEF-H1 in HRAS^{V12}-transformed NIH 3T3 cells using two distinct GEF-H1 lentiviral hairpins (Figure 3A), which resulted in increased apoptosis as measured by caspase 3 cleavage (Figure 3B). We also observed that stable depletion of GEF-H1 suppressed anchorage-independent growth by 90% compared with parental HRAS^{V12}-transformed cells or transformed cells expressing a nontargeting hairpin (Figures 3C and S2A).

To address the role of GEF-H1 in supporting tumor formation of HRAS^{V12}-transformed NIH 3T3 cells, we generated subcutaneous tumor xenografts in NCr nude mice. Parental and shGFP-expressing cells formed tumors within 10 days of injection, while GEF-H1-depleted cells demonstrated attenuated tumor growth (Figures 3D, 3E and S2B). Moreover, GEF-H1-depleted tumors exhibited increased caspase 3 cleavage relative to parental and hairpin controls (Figure 3F). To further examine the role of GEF-H1 in HRAS^{V12}-mediated cell survival, we monitored the behavior of MEFs derived from *Arhgef2* knockout mice (*Arhgef2*$^{-/-}$) following ectopic expression of HRAS^{V12} (Figure 3G). Extensive cell death was observed in *Arhgef2*$^{-/-}$ compared to wild-type MEFs following HRAS^{V12}

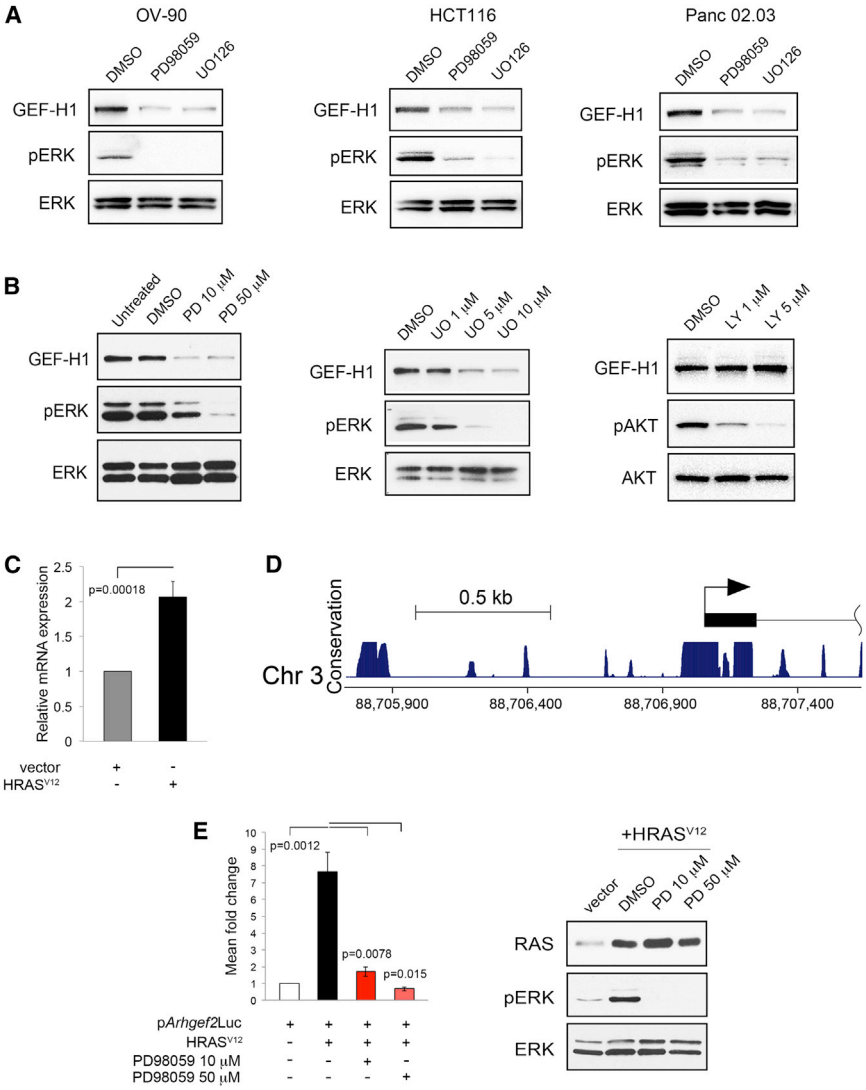

Figure 2. *Arhgef2* Is a Transcriptional Target of the RAS/MAPK Pathway

(A) Immunoblot analysis of GEF-H1 expression in cancer cell lines after treatment with DMSO, PD98059 (30 μM), or UO126 (10 μM) for 48 hr.

(B) $HRAS^{V12}$-transformed NIH 3T3 cells were treated with DMSO, PD98059, UO126, or LY294002 for 48 hr, and GEF-H1 expression was assessed by western blot. pERK and ERK indicate phosphorylated and total ERK, respectively, whereas pAKT and AKT indicate phosphorylated and total AKT, respectively.

(C) The GEF-H1 mRNA level in NIH 3T3 cells expressing vector or T7-$HRAS^{V12}$ was quantified by real-time PCR and normalized to tubulin. Levels are represented as fold change over vector-expressing cells.

(D) Schematic representation of the putative promoter region of murine *Arhgef2* showing the highly conserved transcriptional start site (TSS) from the UCSC genome browser.

(E) p*Arhgef2*Luc was co-transfected with empty vector or T7-$HRAS^{V12}$ expression plasmid and treated with PD98059. Luciferase activity was normalized to renilla expression and is represented as fold change over empty vector-expressing cells (left graph). Lysates were assayed for RAS expression and MAPK activation by western blot (right panel). All data are representative of three independent experiments ± SEM.

expression. Re-expression of GEF-H1 in *Arhgef2*$^{-/-}$ MEFs expressing $HRAS^{V12}$ restored cell viability. These data show that GEF-H1 contributes to $HRAS^{V12}$-mediated cell transformation and cell viability in vitro and in vivo.

GEF-H1 Induction and Dependency in $BRAF^{V600E}$-Expressing Cell Lines

Because OV-90 carries the activating *BRAF*^{V600E} mutation (Estep et al., 2007), we queried whether $BRAF^{V600E}$ similarly induced GEF-H1 protein expression. We found that GEF-H1 protein levels were increased in $BRAF^{V600E}$-transformed NIH 3T3 cells and were sensitive to MEK inhibition (Figures S2C and S2D). Moreover, GEF-H1 expression in the human melanoma cell line A375, which carries an endogenous *BRAF*^{V600E} mutation, was suppressed following MEK inhibition (Figure S2E). $BRAF^{V600E}$ expression also induced a 4.6-fold increase in the normalized *Arhgef2* promoter-mediated reporter expression compared to NIH 3T3 cells expressing the *Arhgef2* promoter alone, which was suppressed with MEK inhibition (Figure S2F). Lastly, knockdown of GEF-H1 induced cell death in $BRAF^{V600E}$-transformed cells (Figures S2G and S2H). These data indicate that the induction of GEF-H1 expression and GEF-H1-dependent cell survival extends to other oncogenes that activate the MAPK pathway.

GEF-H1 Is Necessary for Optimal MAPK Pathway Activation in Response to $HRAS^{V12}$

We next sought to investigate the mechanism underlying the contribution of GEF-H1 to $HRAS^{V12}$-mediated cellular transformation. We compared the levels of Rho-GTP in control and GEF-H1 knockdown cells expressing $HRAS^{V12}$ but found no change in Rho-GTP levels (Figure S3A and S3B), demonstrating that a change in Rho-GTP cannot account for the contribution of GEF-H1 in $HRAS^{V12}$-mediated transformation. We therefore investigated whether elevated levels of GEF-H1 affected the signaling characteristics of upstream components of the RAS/MAPK pathway as part of a potential positive feedback mechanism. We expressed $HRAS^{V12}$ in MEFs harboring stable knockdown of GEF-H1 and probed lysates for phosphorylated forms of MEK1/2 and ERK1/2 to assess MAPK pathway activity. MEK1/2 and ERK1/2 were highly phosphorylated in $HRAS^{V12}$-expressing MEFs (Figure 4A, lane 2), but, surprisingly, MEK1/2 and ERK1/2 phosphorylation was significantly reduced in GEF-H1-depleted cells (Figure 4A, lanes 4 and 6). Expression of an shRNA-resistant GEF-H1 (rGEF-H1) restored MEK1/2 and ERK1/2 phosphorylation in response to $HRAS^{V12}$ expression in GEF-H1 knockdown MEFs (Figure 4A, lane 7). A similar defect in $HRAS^{V12}$-mediated ERK1/2 phosphorylation was seen in

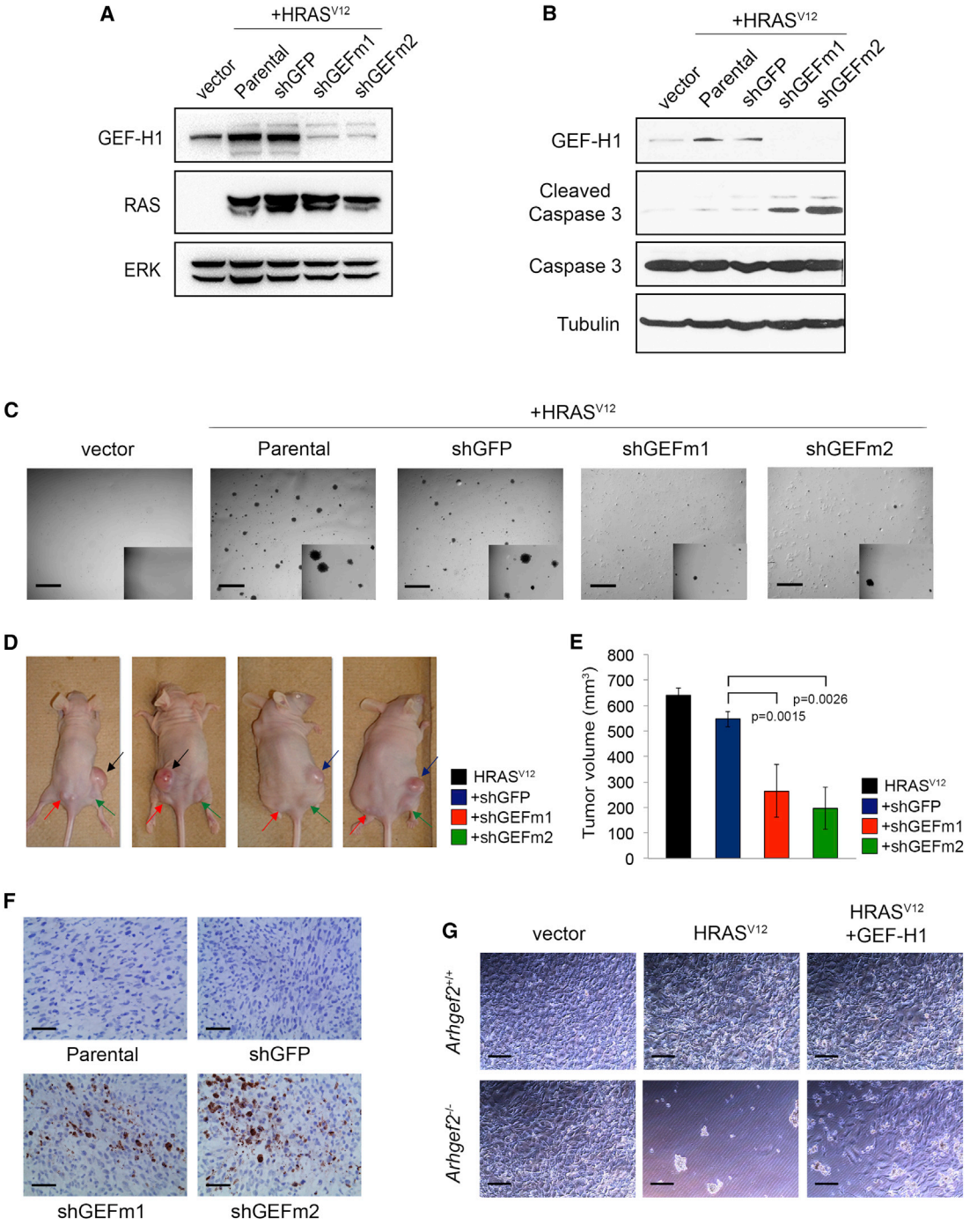

Figure 3. GEF-H1 Contributes to Cell Survival and Growth in HRAS^{V12}-Transformed Cells

(A) GEF-H1 protein levels in NIH 3T3 cells expressing vector, HRAS^{V12}, or HRAS^{V12} with a control hairpin (shGFP) or two distinct murine GEF-H1 shRNAs (shGEFm1 and shGEFm2).

(B) Cells described in (A) were probed for caspase 3 cleavage by western blot 5 days after infection with lentiviral hairpins. Tubulin served as a protein loading control.

(C) Representative images of cell lines described in (A) grown for 10 days in 0.3% agar to form colonies. Scale bars, 200 μm.

(D) Photographs of NCr nude mice 14 days after subcutaneous injection of cells described in (A).

(E) Final mean tumor volumes are shown in (D). Results are the combination of four independent experiments (n = 21 tumors). Error bars indicate ± SEM.

(F) Immunohistochemistry of NIH 3T3-HRAS^{V12} tumor sections stained for cleaved caspase 3. Four tumors were sampled from two independent experiments. Scale bars, 100 μm.

(G) Bright field images of wild-type or *Arhgef2*$^{-/-}$ MEFs expressing eGFP, eGFP-HRAS^{V12}, or eGFP-HRAS^{V12} and Flag-GEF-H1 4 days after transfection and selection. Scale bars, 100 μm.

See also Figure S2.

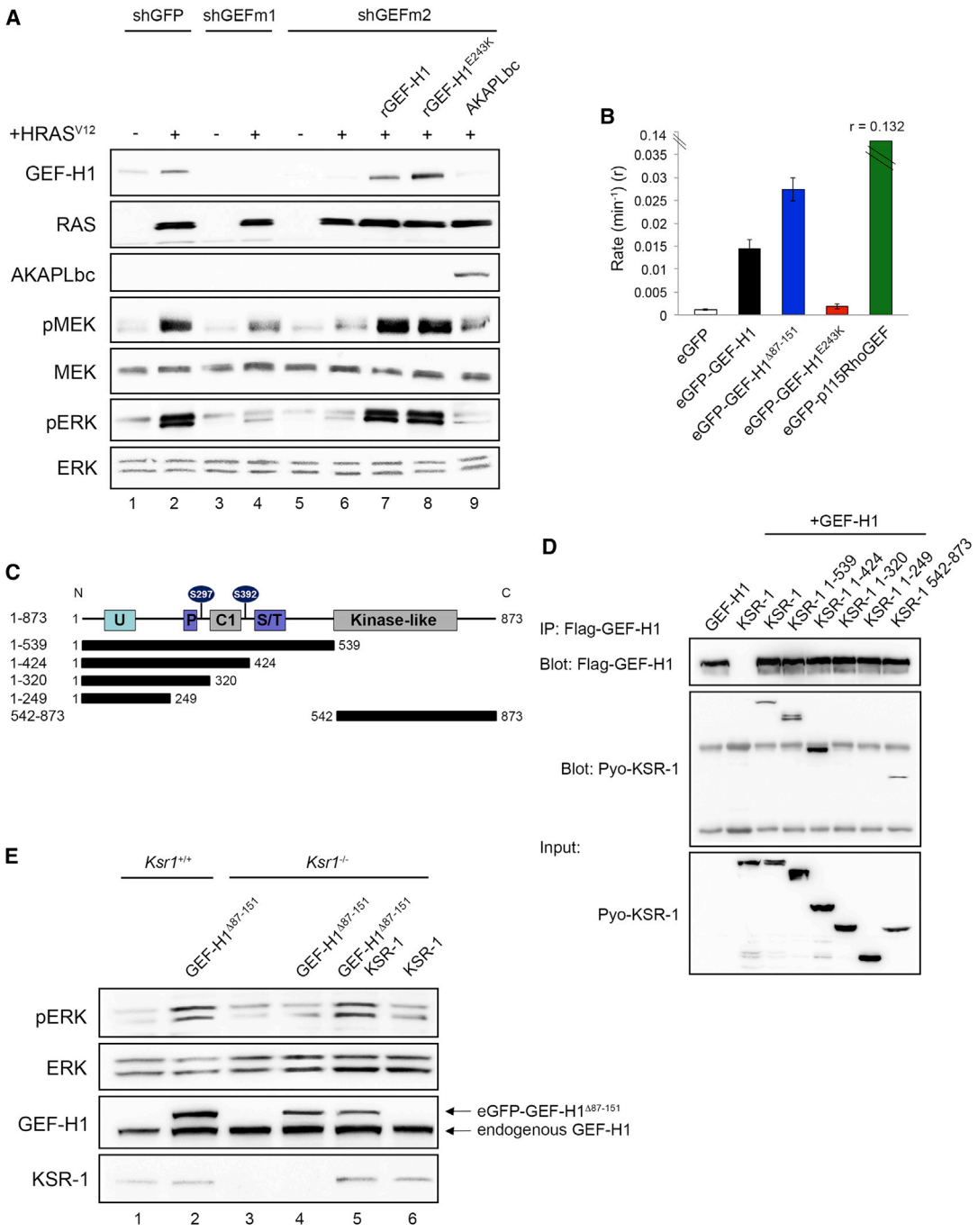

Figure 4. GEF-H1 Is Necessary for Optimal MAPK Pathway Activation in Response to HRAS^{V12}

(A) MEFs stably expressing shGFP, shGEFm1, or shGEFm2 were transfected with empty vector or HRAS^{V12} and probed for pERK or pMEK by western blot. shGEFm2-expressing cells were co-transfected with HRAS^{V12} and Flag-rGEF-H1, Flag-rGEF-H1^{E243K}, or Flag-AKAPLbc. Expression of plasmids was confirmed by immunoblotting with anti-GEF-H1, anti-RAS, or anti-Flag (AKAPLbc) antibodies.

(B) Real-time NMR measurement of RhoA nucleotide exchange rates in lysates from HEK293T cells expressing eGFP, eGFP-GEF-H1, eGFP-GEF-H1$^{\Delta 87–151}$, eGFP-GEF-H1^{E243K}, or eGFP-p115RhoGEF. Graphical representation of eGFP-p115RhoGEF-induced nucleotide exchange rate is not to scale as indicated by breaks in graph, because the rate was 9.4-fold over eGFP-GEF-H1 (r = 0.132 versus r = 0.014). Data are representative of three independent experiments ± SD.

(C) Schematic representation of KSR-1 constructs used in (D).

(D) Pyo-tagged KSR-1 constructs were coexpressed with Flag-GEF-H1 in HEK293T cells. Protein complexes were immunoprecipitated with anti-Flag antibody, and proteins were detected by immunoblotting with anti-KSR-1 or anti-Flag antibodies.

(E) MEFs were transfected with vector or eGFP-GEF-H1$^{\Delta 87–151}$, and *Ksr1*$^{-/-}$ MEFs were transfected with vector, eGFP-GEF-H1$^{\Delta 87–151}$, eGFP-GEF-H1$^{\Delta 87–151}$ and Pyo-KSR-1, or Pyo-KSR-1 alone and assayed for pERK by western blot. GEF-H1 and KSR-1 expression was determined by western blot.

See also Figure S3.

Arhgef2$^{-/-}$ MEFs, which was restored by GEF-H1 expression (Figure S3C, lanes 4 and 5).

To determine the specificity of GEF-H1-dependent MAPK pathway activation, we attempted to rescue the GEF-H1 knockdown phenotype by expressing either AKAP-Lbc, the closest GEF family member to GEF-H1, or p115 RhoGEF, another RhoGEF family member. Neither AKAP-Lbc (Figure 4A, lane 9) nor p115 RhoGEF (Figure S3C, lane 7) rescued MEK1/2 and ERK1/2 phosphorylation in response to acute HRAS^{V12} expression in GEF-H1 knockdown or *Arhgef2*$^{-/-}$ MEFs, respectively, despite 9-fold greater catalytic activity of p115RhoGEF compared to GEF-H1 (Figure 4B). To investigate whether GEF-H1-mediated MAPK pathway activation was dependent on its GEF activity, we coexpressed a catalytically inactive, shRNA-resistant form of GEF-H1 (rGEF-H1^{E243K}, Figure 4B) with HRAS^{V12} in MEFs depleted of endogenous GEF-H1 and found that MEK1/2 and ERK1/2 phosphorylation was fully restored (Figure 4A, lane 8). These findings were confirmed in *Arhgef2*$^{-/-}$ MEFs (Figure S3C, lane 6). These data show that GEF-H1 potentiates the HRAS^{V12}/MAPK pathway in a manner independent of its GEF activity.

GEF-H1 Is a Component of the KSR-1 Complex and Is Required for the Dephosphorylation of the Negative Regulatory Site of KSR-1

Given that GEF-H1 catalytic activity is dispensable for HRAS^{V12}-dependent MAPK pathway activation, we hypothesized that GEF-H1 may be providing a scaffold function for components of the MAPK pathway. We investigated whether GEF-H1 could form a complex with KSR-1, the major scaffold for the MAPK pathway. We detected an interaction between endogenous GEF-H1 and endogenous KSR-1 in GEF-H1 immunoprecipitates from wild-type, but not *Arhgef2*$^{-/-}$, MEFs (Figure S3D). Similarly, in an overexpression system, we detected an interaction between KSR-1 and a mutant of GEF-H1 deleted of the negative regulatory sequences between amino acids 87–151 and unbound from microtubules (GEF-H1$^{\Delta 87-151}$, Meiri et al., 2012) (Figure S3E). To discern which domains of KSR-1 interact with GEF-H1, we analyzed Flag-GEF-H1 immune complexes from cells that expressed full-length or a series of Pyo-tagged KSR-1 deletions (Figure 4C). We found that full-length KSR-1, KSR-1 (1–539), KSR-1(1–424), and KSR-1(542–873) interacted with full-length GEF-H1 (Figure 4D). These data show that KSR-1 can form a complex with GEF-H1 and that both the C1 domain and the kinase domain of KSR-1 contribute to GEF-H1 binding.

We next sought to determine whether ERK1/2 activation by GEF-H1 was dependent on KSR-1. Expression of the active GEF-H1$^{\Delta 87-151}$ mutant (Figure 4B) in wild-type MEFs induced strong ERK1/2 phosphorylation even in the absence of HRAS^{V12} expression (Figure 4E, lane 2), whereas *Ksr1*$^{-/-}$ MEFs were resistant to GEF-H1$^{\Delta 87-151}$-induced ERK1/2 phosphorylation (Figure 4E, lane 3 and 4). Re-expression of KSR-1 restored GEF-H1$^{\Delta 87-151}$-induced ERK1/2 phosphorylation in *Ksr1*$^{-/-}$ cells (Figure 4E, lane 5), whereas re-expression of KSR-1 in the absence of GEF-H1$^{\Delta 87-151}$ alone had little effect on ERK1/2 phosphorylation (Figure 4E, lane 6). These data confirm that GEF-H1 requires KSR-1 to positively regulate ERK1/2 activation.

Platelet-derived growth factor (PDGF) or HRAS^{V12} induce the dephosphorylation of KSR-1 at S392 and its subsequent translocation from the cytoplasm to the plasma membrane (Ory et al., 2003). We therefore examined the requirement of GEF-H1 for PDGF-induced KSR-1 membrane translocation (Figure 5A). In 22% (21 of 97) of wild-type cells, KSR-1 translocated from the cytoplasm to the plasma membrane in a PDGF-dependent manner (Figure 5A, columns 1 and 2; Figure S4A). By contrast, only 3.5% of cells (3 of 87) underwent PDGF-dependent membrane translocation in *Arhgef2*$^{-/-}$ cells (Figure 5A, columns 3 and 4; Figure S4A), a defect that was rescued by the expression of wild-type GEF-H1 (Figure 5A, columns 5 and 6; Figure S4A). Because translocation of KSR-1 to the plasma membrane requires dephosphorylation of S392, we queried whether the S392A point mutant form of KSR-1 could rescue the dependence on GEF-H1 for translocation to the plasma membrane. We expressed wild-type KSR-1 or KSR-1^{S392A} in *Arhgef2*$^{-/-}$ cells and found that, in the absence of growth factor stimulation, wild-type KSR-1 was rarely associated with the plasma membrane (9% or 6 of 69 cells, Figures 5B and S4B), whereas KSR-1^{S392A} efficiently localized to the plasma membrane even in the absence of GEF-H1 (37% or 28 of 76 cells) (Figure 5B, columns 1 and 2; Figure S4B). These data show that GEF-H1 is required for the translocation of KSR-1 to the plasma membrane in a manner that depends on the dephosphorylation of KSR-1 on S392. Re-expression of GEF-H1 and KSR-1 in *Arhgef2*$^{-/-}$ MEFs was insufficient to induce membrane translocation of KSR-1 in the absence of PDGF treatment (6% or 4 of 67 cells) (Figure 5B, column 3; Figure S4B). However, the requirement for growth factor-stimulated KSR-1 translocation to the plasma membrane could be circumvented by the expression of the non-microtubule-associated form of GEF-H1, GEF-H1$^{\Delta 87-151}$ (Meiri et al., 2012), with 30% (21 of 71) of cells exhibiting KSR-1 plasma membrane localization (Figure 5B, column 4; Figure S4B). These data suggest that the growth factor dependence of KSR-1 translocation to the plasma membrane is contingent on the release of GEF-H1 from the microtubule array. Importantly, we found that the endogenous interaction of GEF-H1 and KSR-1 was induced between 5–20 min of PDGF stimulation, correlating with their translocation to the plasma membrane (Figure 5C). These data suggest that endogenous complex formation between GEF-H1 and KSR-1 occurs at the plasma membrane in response to PDGF treatment.

To clarify whether the dependence of HRAS^{V12} on GEF-H1 for cell survival was mediated through KSR-1, we measured cell viability following ectopic expression of wild-type KSR-1 or KSR-1^{S392A} with HRAS^{V12} in *Arhgef2*$^{-/-}$ MEFs and found that only KSR-1^{S392A} restored cellular viability (Figures 5D and 5E). These data provide genetic evidence that dephosphorylation of the negative regulatory site S392 on KSR-1 is the critical target downstream of GEF-H1 that supports cell survival in HRAS^{V12}-transformed cells.

To determine whether GEF-H1 regulation of the HRAS^{V12}/MAPK cascade is coupled to the dephosphorylation of KSR-1, we asked whether wild-type KSR-1 or KSR-1^{S392A} could restore HRAS^{V12}-induced ERK1/2 phosphorylation in the absence of GEF-H1. HRAS^{V12} expression induced ERK1/2 phosphorylation in control hairpin-expressing MEFs, but not in cells depleted of GEF-H1 (Figure 5F, lanes 2 and 4). High expression of rGEF-H1 in GEF-H1-depleted cells greatly enhanced ERK1/2 activation in response to HRAS^{V12}, supporting the model that increased levels of GEF-H1 result in amplification of the MAPK

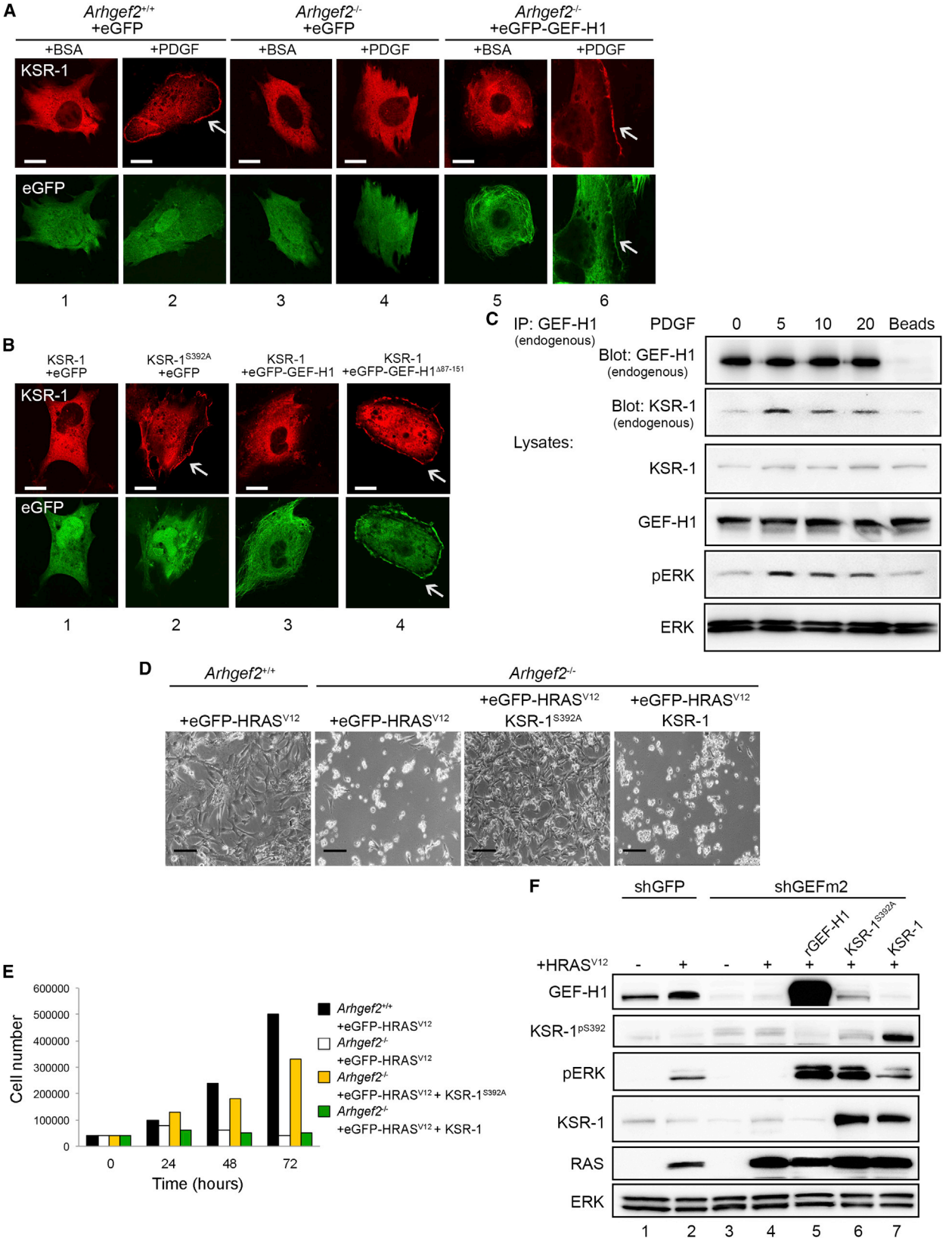

(legend on next page)

cascade (Figure 5F, lane 5). Expression of KSR-1^{S392A} efficiently restored HRAS^{V12}-mediated ERK1/2 phosphorylation in GEF-H1 knockdown cells compared to wild-type KSR-1 (Figure 5F, lanes 6 and 7). These data demonstrate that dephosphorylation of KSR-1 S392 is sufficient to overcome the GEF-H1-dependence of HRAS^{V12}-mediated ERK1/2 activation.

GEF-H1 Is Required for PP2A-Mediated Dephosphorylation of KSR-1

In an independent study, we identified GEF-H1 as a PP2A interacting partner in a proteomic screen designed to probe for proteins that bound to the PP2A catalytic subunit (D.M., C.B.M., J.L., M. Mullin, A.-C.G., M.I., and R.R., unpublished data) and found that GEF-H1 interacts with the B' regulatory PP2A subunits (PPP2R5A, PPP2R5B, and PPP2R5E). We hypothesized that GEF-H1 may function as a bridge between KSR-1 and PP2A to control KSR-1 S392 dephosphorylation. First, we confirmed the previously published data showing an interaction between KSR-1 and the B' regulatory PP2A subunits (Figure 6A) (Ory et al., 2003). We observed that GEF-H1 bound to the same PP2A subunits that interacted with KSR-1 (Figure 6A). We next determined the regions of GEF-H1 involved in PP2A and KSR-1 binding by expressing deletion mutants of GEF-H1 (Figure 6B) and probing for the catalytic subunit of PP2A and KSR-1 in GEF-H1 immune complexes (Figure 6C). Analysis of GEF-H1 immunoprecipitates revealed that endogenous KSR-1 interacted with full-length GEF-H1, GEF-H1(236–572), and GEF-H1(236–433). These results localize the binding site for KSR-1 to the DH domain of GEF-H1, while endogenous PP2Ac binds to the GEF-H1 PH domain (Figure 6C). These data show that KSR-1 and PP2A bind to distinct sites on GEF-H1 and suggest that GEF-H1 may function to bridge PP2A to KSR-1.

To determine whether GEF-H1 acts as a bridge to link KSR-1 to PP2A, we stably infected human embryonic kidney 293T (HEK293T) cells expressing the PP2A B' subunit with an shRNA targeting GEF-H1 and probed PP2A immunoprecipitates for endogenous KSR-1 (Figure 6D). KSR-1 was detected in immune complexes of PP2A B' subunits in shGFP-expressing cells, but not those depleted of GEF-H1. Thus, the interaction between KSR-1 and PP2A is dependent on GEF-H1. These data support a model whereby GEF-H1 provides a bridging function to recruit the PP2A B' subunits required for the dephosphorylation of the negative regulatory S392 site on KSR-1 and activation of the MAPK pathway.

Given that dephosphorylation of KSR-1 on S392 is induced in response to PDGF and oncogenic RAS, we sought to determine whether the interaction between GEF-H1 and KSR-1 was similarly regulated. We isolated Flag-PPP2R5E immune complexes from HEK293T cells and probed them for the presence of GEF-H1 and KSR-1 after PDGF treatment (Figure 6E). Although GEF-H1 and KSR-1 were not detectable in PPP2R5E immune complexes in starved cells, both GEF-H1 and KSR-1 were recruited to PPP2R5E immune complexes after 5 min of PDGF stimulation and disappeared after 15 min (Figure 6E). Moreover, induction of oncogenic HRAS with 4-OHT induced a protein complex composed of endogenous KSR-1, GEF-H1, and PPP2R5E proteins after 20 min and extending to 90 min following RAS activation (Figure S5). These data show that PDGF or HRAS^{V12} induce the formation of a KSR-1, GEF-H1, and PP2A protein complex. Moreover, the complex appears to be temporally regulated, suggesting the presence of feedback mechanisms that attenuate its assembly even with constitutive activation of the pathway.

GEF-H1 Is Important for the Growth of RAS Mutant Pancreatic Tumor Xenografts

Over 90% of human pancreatic ductal adenocarcinomas (PDACs) harbor activating mutations in *KRAS* (Smit et al., 1988). We evaluated whether GEF-H1 expression was increased in PDAC by immunohistochemistry on pancreatic tissue microarrays (TMAs). We probed tissue sections of 14 normal pancreatic ducts, 32 PanIN-1 (A and B) lesions, 9 PanIN-2 and IN-3 lesions, and 14 PDAC tumor samples for GEF-H1 expression using a monoclonal antibody against GEF-H1 (Figure 7A). Normal pancreatic ducts and PanIN-1 lesions did not express GEF-H1, whereas greater than 90% (21 out of 23) of the more advanced histologic grades expressed GEF-H1 (Figures 7A and S6A). These data demonstrate that GEF-H1 expression is positively correlated with neoplastic progression of pancreatic tumors. Treatment of the PDAC cell line PANC-1, harboring a *KRAS*^{D12} mutation, with MEK inhibitors PD98059 or UO126 resulted in reduced GEF-H1 levels (Figure S6B). Together, these data show that GEF-H1 expression is increased in PDAC cells in a manner that is dependent on MAPK pathway activation.

To determine whether GEF-H1 was necessary for MAPK pathway activation in PDAC cells, we knocked down GEF-H1 in PANC-1 cells and observed increased KSR-1 S392 phosphorylation and a corresponding decrease in ERK1/2

Figure 5. KSR-1 Signals through GEF-H1 in Response to PDGF and Oncogenic RAS

(A) Wild-type or *Arhgef2*$^{-/-}$ MEFs were transfected with eGFP or eGFP-GEF-H1 and treated with BSA or 25 ng/ml PDGF for 10 min and fixed and stained for endogenous KSR-1. Arrows indicate KSR-1 plasma membrane localization and eGFP-GEF-H1 localization. Scale bars, 20 μm. Images are representative of four independent experiments.

(B) *Arhgef2*$^{-/-}$ MEFs were co-transfected with KSR-1 or KSR-1^{S392A} and eGFP, eGFP-GEF-H1, or eGFP-GEF-H1$^{\Delta 87–151}$ and stained for endogenous KSR-1. Arrows and scale bars are as in (A), and images are representative of four independent experiments.

(C) HEK293T cells were starved for 12 hr and treated with BSA or 25 ng/ml PDGF for 5, 10, or 20 min. Endogenous GEF-H1 immune complexes were isolated and probed for the presence of endogenous KSR-1. Lysates were probed for total levels of GEF-H1 and KSR-1. pERK and ERK reflect the temporality of MAPK pathway activation and total protein levels, respectively.

(D) Representative bright field images of wild-type or *Arhgef2*$^{-/-}$ MEFs expressing eGFP-HRAS^{V12}, eGFP-HRAS^{V12} + Pyo-KSR-1, or eGFP-HRAS^{V12} + Pyo-KSR-1^{S392A} 72 hr after transfection. Scale bars, 100 μm.

(E) Quantification of the number of viable cells described in (D) 24, 48, and 72 hr after transfection; 4 × 10^4 cells were plated at time 0.

(F) MEFs stably expressing shGFP or shGEFm2 were transfected with vector, HRAS^{V12}, or co-transfected with HRAS^{V12} and Flag-rGEF-H1, Pyo-KSR-1^{S392A}, or Pyo-KSR-1. KSR-1 S392 phosphorylation was assessed with a pS392-specific KSR-1 antibody.

See also Figure S4.

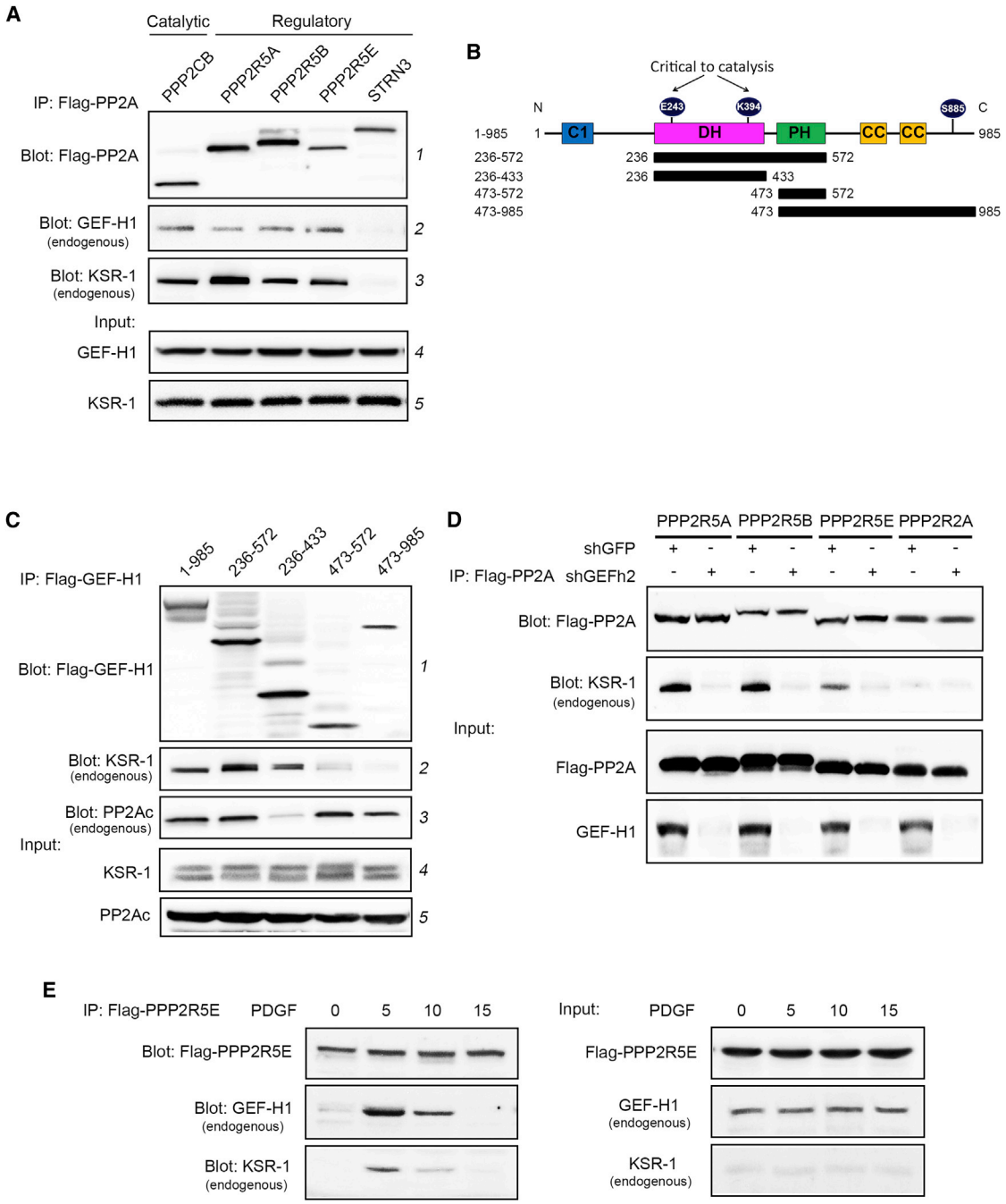

Figure 6. GEF-H1 Is Required for PP2A-Mediated Dephosphorylation of KSR-1 on S392

(A) Flag-PP2A immune complexes were isolated from stable Flag-PP2A catalytic and regulatory subunit-expressing HEK293T cells using anti-Flag antibodies. Flag-PP2A complexes were probed for endogenous GEF-H1 and endogenous KSR-1 (rows 2 and 3). Total expression levels of GEF-H1 and KSR-1 in lysates are shown in rows 4 and 5.

(B) Schematic representation of GEF-H1 constructs used in (C).

(C) Flag-tagged truncated variants of GEF-H1 were expressed in HEK293T cells, and protein complexes were immunoprecipitated with anti-Flag antibodies. Lysates were probed with anti-KSR-1 or anti-PP2Ac antibodies.

(D) HEK293T cells stably expressing Flag-tagged PP2A regulatory subunits were infected with shGFP or shGEFh2 lentiviruses. Flag-PP2A subunits were immunopurified with anti-Flag (row 1) and probed for endogenous KSR-1 (row 2). Flag-PP2A subunit expression (row 3) and GEF-H1 knockdown (row 4) were confirmed by immunoblotting lysates with Flag and GEF-H1 antibodies, respectively.

(E) HEK293T cells stably expressing Flag-PPP2R5E were treated with 25 ng/ml PDGF for 0, 5, 10, or 15 min. Flag-PPP2R5E immune complexes were isolated with anti-Flag antibodies and probed for the presence of endogenous GEF-H1 and KSR-1 (left panel). Lysates were probed for total levels of Flag-PPP2R5E, endogenous GEF-H1 and KSR-1 (right panel).

See also Figure S5.

phosphorylation compared with control hairpin-expressing cells (Figure 7B). Expression of shRNA-resistant GEF-H1$^{\Delta 87-151}$ restored the basal levels of phosphorylated KSR-1 and ERK1/2 in GEF-H1-depleted cells (Figure 7B). These data indicate that GEF-H1 is both necessary and sufficient for KSR-1 S392 dephosphorylation and ERK1/2 activation in PDAC cells harboring endogenous RAS mutations. Expression of KSR-1^{S392A}, but not wild-type KSR-1, corrected the defect in the phosphorylated ERK levels in GEF-H1 knockdown cells, showing that active KSR-1 can circumvent the need for GEF-H1 in PANC-1 cells (Figure 7B).

We tested the contribution of GEF-H1 to the in vitro cell growth of four human KRAS mutant pancreatic cancer derived cell lines including PANC-1 Panc 08.13, Panc 04.03, and PL-45 (Figures S6C–S6F). These cell lines displayed varying sensitivity to GEF-H1 depletion for cell growth (a 50%, 90%, 80%, and 65% reduction, respectively) compared to control hairpin-expressing cells. Of the six pancreatic lines that we had tested, we examined the contribution of GEF-H1 to tumor growth in three of these lines, PANC-1 (*KRAS*^{D12}), HPAF-II (*KRAS*^{D12}), and BxPC3 (wild-type *KRAS*), in immune-deficient mice. PANC-1 and HPAF-II cells exhibited profound attenuation of tumor growth relative to control hairpin cells (Figures 7C, S6G, and S6H). The tumor growth of BxPC3 cells was not affected by depletion of GEF-H1, highlighting the dependency of oncogenic RAS on GEF-H1 (Figures 7C and S6I). In addition, increased tumor-associated caspase 3 cleavage was observed in PANC-1 xenografts (Figure S6J). Collectively, our data demonstrate an amplifying feedback loop involving GEF-H1 in the RAS/MAPK pathway across a variety of cell types expressing different mutant RAS family members. These data support the model that GEF-H1 is important for the growth of tumor cells harboring activating mutations in RAS.

DISCUSSION

Signaling through the RAS/MAPK pathway is gated by KSR-1, a highly conserved scaffold protein that ensures strict spatiotemporal regulation of ERK activation. Genetic studies have demonstrated a critical requirement of KSR-1 for growth factor-mediated signaling through the RAS/MAPK pathway (Sieburth et al., 1999; Lozano et al., 2003) and the formation of HRAS^{V12}-dependent tumors (Xiao et al., 2010). The requirement of KSR-1 in HRAS^{V12}-mediated transformation is strictly dependent on the dephosphorylation of KSR-1 at S392 by PP2A (Razidlo et al., 2004). In this study, we provide a mechanistic explanation of how the B' subunit is recruited to the PP2A/KSR-1 complex and uncover a positive feedback loop involving the RhoGEF GEF-H1 that is necessary for HRAS^{V12}-mediated transformation. We show that *Arhgef2* is a direct transcriptional target of the RAS/MAPK pathway, and its elevated protein expression is similarly responsive to oncogenic BRAF and H-, K-, and NRAS family members. We demonstrate that GEF-H1 contributes to the growth and survival of BRAF^{V600E} and HRAS^{V12}-transformed NIH 3T3 cells and PDAC xenografts. We anticipate that there may be examples of escape mechanisms whereby some RAS mutant tumors no longer depend on the GEF-H1 amplifying loop, which will be an area of future investigation.

The discovery that a RhoGEF is involved in a positive feedback loop for the MAPK pathway suggests a model whereby amplification of the MAPK pathway could be coupled to signal diversification through the activation of RhoA, a known component of the RAS transformation program (Qiu et al., 1995; Prendergast et al., 1995; Sahai et al., 2001; Chen et al., 2003). Our data suggest that oncogenic RAS induces RhoA-GTP independently of GEF-H1, a finding consistent with the previously reported model that a decrease in p190RhoGAP activity, rather than an increase in total cellular RhoGEF activity, controls RhoA-GTP levels in HRAS^{V12}-transformed cells (Chen et al., 2003). The observation that overexpression of GEF-H1 is sufficient to increase MEK1/2 and ERK1/2 phosphorylation raises the possibility that the oncogenic potential of GEF-H1 is mediated through its capacity to increase cellular Rho-GTP levels and/or activate the MAPK pathway.

An important implication that follows from this study is the possibility that mitogenic signals conveyed through the MAPK pathway might be coupled to microtubule function through GEF-H1, thereby coordinating growth signals with changes in cell shape, migration, and/or morphogenesis. We show that the mutant GEF-H1$^{\Delta 87-151}$, unable to interact with the microtubule array, is largely cytoplasmic (Meiri et al., 2012) and is able to induce KSR-1 membrane translocation and ERK1/2 phosphorylation in the absence of either PDGF or oncogenic RAS. These findings suggest that the release of GEF-H1 from microtubules links HRAS^{V12} to KSR-1 function. This idea is supported by the observations that depolymerization of microtubules potently activates components of the MAPK pathway through currently unknown mechanisms (Birukova et al., 2005; Guo et al., 2012; Hayne et al., 2000). Active HRAS contributes to microtubule instability that may promote the invasive behavior of transformed cells and reinforce the GEF-H1 positive feedback loop on the MAPK pathway (Harrison and Turley, 2001). In addition, ERK phosphorylation and activation of GEF-H1 (Fujishiro et al., 2008) might trigger its release from microtubules, where it can interact with cytosolic KSR-1. The signaling events that coordinate the spatial coupling of GEF-H1 with cytosolic KSR-1 remain to be elucidated.

The identification of GEF-H1 as a component of the RAS signaling circuitry is part of an emerging role of RhoGEFs in RAS signaling. TIAM1, a Rac exchange factor, is directly activated by RAS-GTP through a RAS binding motif in its N terminus and is required for RAS-induced skin tumors (Lambert et al., 2002; Malliri et al., 2002). The RhoGEF AKAP-Lbc was shown to couple PKA to KSR-1 through its A-kinase anchoring protein scaffold function (Smith et al., 2010). GEF-H1 may also be important in other genetic contexts, because it has been reported to contribute to the growth and survival of cell lines harboring stabilizing p53 mutations and those expressing the oncogene hPTTG1 (Mizuarai et al., 2006; Liao et al., 2012).

The GEF-H1-mediated feedback loop adds to a growing number of other feedback loops that control flux through the MAPK pathway. ERK1/2-dependent phosphorylation of upstream components SOS, RAF, and EGFR (Buday et al., 1995; Porfiri and McCormick, 1996; Dougherty et al., 2005; Ritt et al., 2010; Heisermann et al., 1990; Li et al., 2008) dampens further pathway activation, and a second, kinetically slower, negative feedback loop involves the induction of DUSP phosphatases that directly

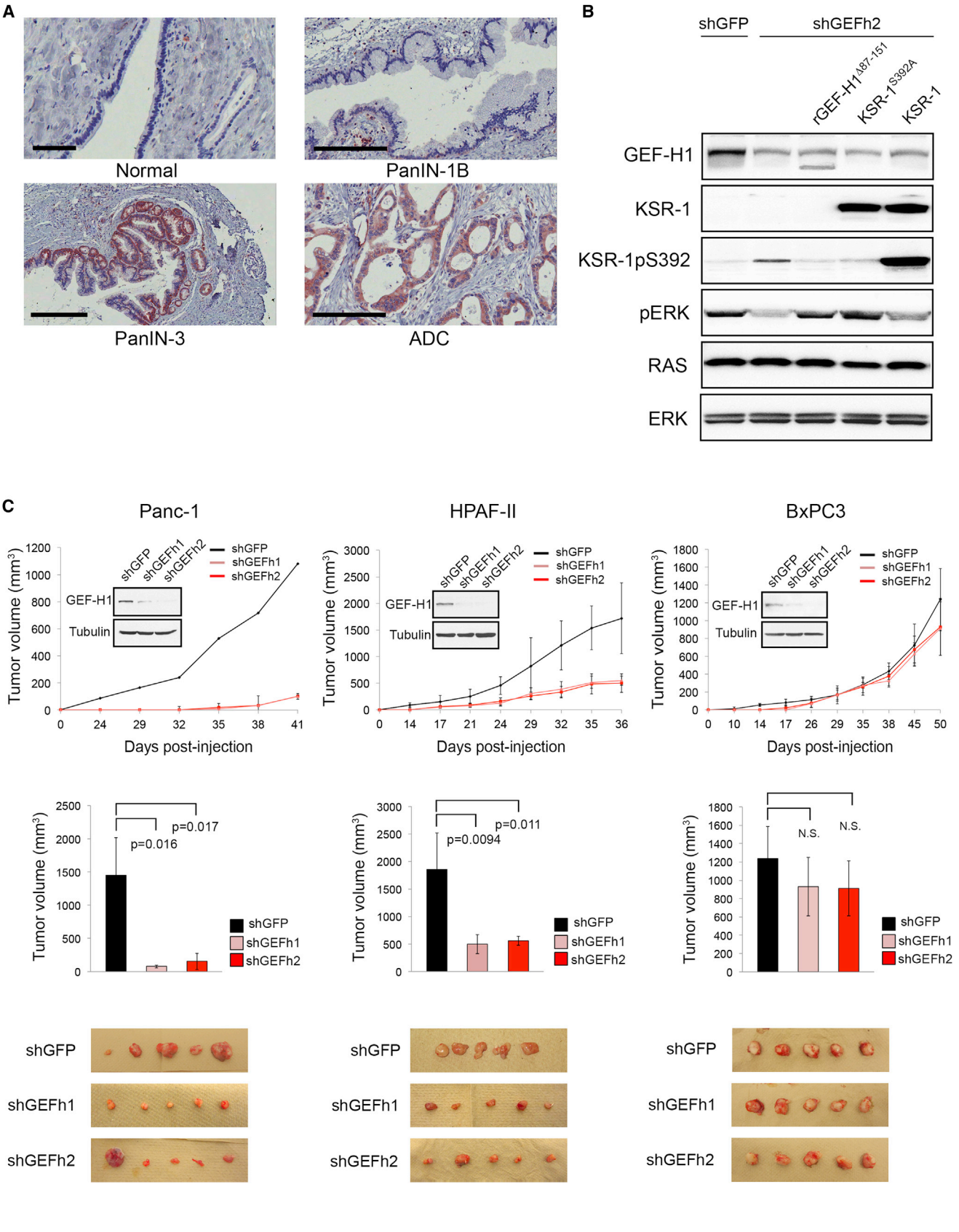

(legend on next page)

dephosphorylate ERK1/2 (Owens and Keyse, 2007). The elaboration of the MAPK pathway with both positive and negative feedback loops ensures that the amplitude and persistence of the MAPK signal is both robust and tunable so as to serve the multiplicity of developmental and mitogenic functions it provides.

In summary, we have found that the induction of GEF-H1 in RAS mutant cells amplifies MAPK signaling and contributes to pancreatic tumor xenograft growth. The identification of GEF-H1 as a component of a positive amplifying loop critical for $HRAS^{V12}$-mediated transformation therefore provides mechanistic insight into the manifold features of the transformation program activated by mutant RAS in human cancers.

EXPERIMENTAL PROCEDURES

Animal Studies

All animal studies were carried out using protocols that have been approved by the University Health Network Animal Care Committee. Detailed experimental procedures are provided in Supplemental Experimental Procedures.

Cell Treatments

ER:$HRAS^{V12}$ MEFs were starved in DMEM containing 0% FBS for 16 hr then treated with 100 nM 4-OHT (Sigma). For MEK and PI3K inhibition experiments, cell lines were cultured in complete medium and incubated with PD98059, UO126, or LY294002 (Sigma) diluted in DMSO (Sigma) for 48 hr. For immunofluorescence studies, MEFs were starved for 24 hr in 0% FBS and treated in DMEM containing 10 mM HEPES and 0.5 mg/ml fatty acid-free BSA (A8806, Sigma). PDGF (Sigma) was suspended in HBSS containing 0.5 mg/ml fatty acid-free BSA and 20 mM HEPES to a stock concentration of 1 μM.

Luciferase Reporter Assays

The regulatory sequence of murine *Arhgef2* (nucleotides 62–1,968 upstream of the transcription start site) was PCR-amplified from mouse BAC clones and inserted into the pGL3 luciferase vector to generate p*Arhgef2*Luc (Promega, E1910). MEFs or NIH 3T3 cells expressing empty vector, $KRAS^{D12}$, or $BRAF^{V600E}$ were plated in a 24-well plate in triplicate at 7×10^4 cells/well. After 16 hr, cells were cotransfected with 50 ng p*Arhgef2*Luc, empty vector, T7-$HRAS^{V12}$, or T7-$KRAS^{D12}$ expression plasmids and 1 ng phRL-SV40 (Promega) using LipoD293 (SignaGen, SL100668) or Lipofectamine 2000 (Invitrogen) according to the manufacturer's instructions. Twenty four hours after transfection, cells were lysed and assayed for firefly and renilla luciferase activity using the Dual-Luciferase Reporter System (Promega). Where indicated, cells were treated with DMSO, PD98059, UO126, or LY294002 for 16 hr prior to cell lysis.

Immunohistochemistry

In this study, we used a human pancreatic TMA generated in a previously published study (Al-Aynati et al., 2004). The use of this TMA in this study was approved by the University Health Network Research Ethics Board (protocol 04-0018T). Immunohistochemistry was performed using the Biotin-Streptavidin-HRP detection system and a human GEF-H1 antibody (14B11 mouse monoclonal antibody) at 1:500 dilution. To evaluate the expression levels of GEF-H1, staining intensity in the ductal cells or lesions were judged by two pathologists and scored as 2 (strong staining), 1 (weak staining), or 0 (absent staining). For NIH 3T3 xenograft studies, tumor sections were fixed in OCT medium, flash frozen in methylbutanol, and stored at −80°C before being sent for immunohistological processing at Toronto General Hospital's Pathology Department. PDAC xenograft tumors were fixed in 10% formalin, paraffin embedded, and sent for immunohistological processing at the Applied Molecular Profiling Lab (Princess Margaret Hospital, Toronto, Canada). Tumor sections were probed for caspase 3 cleavage using anti-cleaved caspase 3 (Asp 175) antibody (CST 9661).

Promoter Analysis of GEF-H1

Phylogenetic footprinting analysis was performed using mouse and human sequences of *ARHGEF2* (NM_1162383.1 and NM_004723.3, respectively) (Zhang and Gerstein, 2003). Sequences were aligned to the genome with BLAT, where the TSS was ascertained, and DNA 1 kb downstream (3′) and 5 kb upstream (5′) were pulled from the database. The 5 kb and 1 kb segments were analyzed separately using Consite (Sandelin et al., 2004), employing all matrices found in the public Jaspar database.

Statistical Analyses

Values are expressed as means ± SD. Paired Student's t tests (Kirkman, 2006) were performed to determine statistical significance between samples. Experiments were performed at least three times, and means with $p < 0.05$ were considered statistically significant.

See Supplemental Experimental Procedures for descriptions of all other experimental procedures.

SUPPLEMENTAL INFORMATION

Supplemental Information includes Supplemental Experimental Procedures, six figures, and one table and can be found with this article online at http://dx.doi.org/10.1016/j.ccr.2014.01.025.

ACKNOWLEDGMENTS

We gratefully acknowledge Marc Therrien (l'IRIC), D. Morrison (National Cancer Institute), J. Scott (Howard Hughes Medical Institute, University of Washington), J. Downward (London Research Institute), G. Mills (The University of Texas MD Anderson Cancer Centre), and D. Bar-Sagi (Langone Medical Centre) for reagents used in this study. R. Agbanay (UHN) assisted with animal studies and A. Daulat (University of Toronto) assisted with luciferase assays. The authors thank Helen Burston for careful reading of the manuscript. This work was supported by the Canadian Institute for Health Research and a joint grant from the Terry Fox Research Institute and the Ontario Institute for Cancer Research.

Received: March 24, 2013
Revised: November 26, 2013
Accepted: January 23, 2014
Published: February 10, 2014

REFERENCES

Al-Aynati, M.M., Radulovich, N., Riddell, R.H., and Tsao, M.S. (2004). Epithelial-cadherin and beta-catenin expression changes in pancreatic intraepithelial neoplasia. Clin. Cancer Res. *10*, 1235–1240.

Figure 7. GEF-H1 Is Important for the Growth of RAS Mutant Pancreatic Tumor Xenografts

(A) GEF-H1 expression in tissue sections of normal pancreatic ducts, PanIN-1B, PanIN-3, or pancreatic adenocarcinoma (ADC) was determined by immunohistochemistry. GEF-H1 staining is represented in brown. Scale bars, 60 μm (Normal); 200 μm (PanIN-1B); 300 μm (PanIN-3); and 200 μm (ADC).

(B) PANC-1 cells were infected with shGFP or shGEFh2 and transfected with Flag-GEF-$H1^{\Delta 87-151}$, Pyo-KSR-1^{S392A}, or Pyo-KSR-1. Lysates were probed for the indicated proteins by immunoblotting.

(C) Indicated cells were infected with shGFP, shGEFh1, or shGEFh2, and GEF-H1 protein expression was assayed by western blot using tubulin as a loading control (insets). Growth curves of xenografts derived from 2×10^5 cells are depicted in the top row. Final mean tumor volumes are depicted in the middle row, and representative images of dissected tumors from one of two experiments performed per cell line are shown in the bottom row. Data are representative of two independent experiments ± SD of n = 5 tumors per condition. N.S. denotes that statistical difference was not significant (p value > 0.05).

See also Figure S6.

Birukova, A.A., Birukov, K.G., Gorshkov, B., Liu, F., Garcia, J.G., and Verin, A.D. (2005). MAP kinases in lung endothelial permeability induced by microtubule disassembly. Am. J. Physiol. Lung Cell. Mol. Physiol. *289*, L75–L84.

Brecht, M., Steenvoorden, A.C., Collard, J.G., Luf, S., Erz, D., Bartram, C.R., and Janssen, J.W. (2005). Activation of gef-h1, a guanine nucleotide exchange factor for RhoA, by DNA transfection. Int. J. Cancer *113*, 533–540.

Buday, L., Warne, P.H., and Downward, J. (1995). Downregulation of the Ras activation pathway by MAP kinase phosphorylation of Sos. Oncogene *11*, 1327–1331.

Cacace, A.M., Michaud, N.R., Therrien, M., Mathes, K., Copeland, T., Rubin, G.M., and Morrison, D.K. (1999). Identification of constitutive and ras-inducible phosphorylation sites of KSR: implications for 14-3-3 binding, mitogen-activated protein kinase binding, and KSR overexpression. Mol. Cell. Biol. *19*, 229–240.

Chen, J.C., Zhuang, S., Nguyen, T.H., Boss, G.R., and Pilz, R.B. (2003). Oncogenic Ras leads to Rho activation by activating the mitogen-activated protein kinase pathway and decreasing Rho-GTPase-activating protein activity. J. Biol. Chem. *278*, 2807–2818.

Cheng, I.K., Tsang, B.C., Lai, K.P., Ching, A.K., Chan, A.W., To, K.F., Lai, P.B., and Wong, N. (2012). GEF-H1 over-expression in hepatocellular carcinoma promotes cell motility via activation of RhoA signalling. J. Pathol. *228*, 575–585.

Davies, H., Bignell, G.R., Cox, C., Stephens, P., Edkins, S., Clegg, S., Teague, J., Woffendin, H., Garnett, M.J., Bottomley, W., et al. (2002). Mutations of the BRAF gene in human cancer. Nature *417*, 949–954.

Dougherty, M.K., Müller, J., Ritt, D.A., Zhou, M., Zhou, X.Z., Copeland, T.D., Conrads, T.P., Veenstra, T.D., Lu, K.P., and Morrison, D.K. (2005). Regulation of Raf-1 by direct feedback phosphorylation. Mol. Cell *17*, 215–224.

Engers, R., Zwaka, T.P., Gohr, L., Weber, A., Gerharz, C.D., and Gabbert, H.E. (2000). Tiam1 mutations in human renal-cell carcinomas. Int. J. Cancer *88*, 369–376.

Estep, A.L., Palmer, C., McCormick, F., and Rauen, K.A. (2007). Mutation analysis of BRAF, MEK1 and MEK2 in 15 ovarian cancer cell lines: implications for therapy. PLoS ONE *2*, e1279.

Frolov, A., Chahwan, S., Ochs, M., Arnoletti, J.P., Pan, Z.Z., Favorova, O., Fletcher, J., von Mehren, M., Eisenberg, B., and Godwin, A.K. (2003). Response markers and the molecular mechanisms of action of Gleevec in gastrointestinal stromal tumors. Mol. Cancer Ther. *2*, 699–709.

Fujishiro, S.H., Tanimura, S., Mure, S., Kashimoto, Y., Watanabe, K., and Kohno, M. (2008). ERK1/2 phosphorylate GEF-H1 to enhance its guanine nucleotide exchange activity toward RhoA. Biochem. Biophys. Res. Commun. *368*, 162–167.

Greenman, C., Stephens, P., Smith, R., Dalgliesh, G.L., Hunter, C., Bignell, G., Davies, H., Teague, J., Butler, A., Stevens, C., et al. (2007). Patterns of somatic mutation in human cancer genomes. Nature *446*, 153–158.

Guo, X., Zhang, X., Li, Y., Guo, Y., Wang, J., Li, Y., Shen, B., Sun, D., and Zhang, J. (2012). Nocodazole increases the ERK activity to enhance MKP-1expression which inhibits p38 activation induced by TNF-α. Mol. Cell. Biochem. *364*, 373–380.

Gupta, S., Ramjaun, A.R., Haiko, P., Wang, Y., Warne, P.H., Nicke, B., Nye, E., Stamp, G., Alitalo, K., and Downward, J. (2007). Binding of ras to phosphoinositide 3-kinase p110alpha is required for ras-driven tumorigenesis in mice. Cell *129*, 957–968.

Harrison, R.E., and Turley, E.A. (2001). Active erk regulates microtubule stability in H-ras-transformed cells. Neoplasia *3*, 385–394.

Hayne, C., Tzivion, G., and Luo, Z. (2000). Raf-1/MEK/MAPK pathway is necessary for the G2/M transition induced by nocodazole. J. Biol. Chem. *275*, 31876–31882.

Heisermann, G.J., Wiley, H.S., Walsh, B.J., Ingraham, H.A., Fiol, C.J., and Gill, G.N. (1990). Mutational removal of the Thr669 and Ser671 phosphorylation sites alters substrate specificity and ligand-induced internalization of the epidermal growth factor receptor. J. Biol. Chem. *265*, 12820–12827.

Jacobs, D., Glossip, D., Xing, H., Muslin, A.J., and Kornfeld, K. (1999). Multiple docking sites on substrate proteins form a modular system that mediates recognition by ERK MAP kinase. Genes Dev. *13*, 163–175.

Janssens, V., and Goris, J. (2001). Protein phosphatase 2A: a highly regulated family of serine/threonine phosphatases implicated in cell growth and signalling. Biochem. J. *353*, 417–439.

Kirkman, T.W. (2006). Statistics to use. http://www.physics.csbsju.edu/stats.

Lambert, J.M., Lambert, Q.T., Reuther, G.W., Malliri, A., Siderovski, D.P., Sondek, J., Collard, J.G., and Der, C.J. (2002). Tiam1 mediates Ras activation of Rac by a PI(3)K-independent mechanism. Nat. Cell Biol. *4*, 621–625.

Li, X., Huang, Y., Jiang, J., and Frank, S.J. (2008). ERK-dependent threonine phosphorylation of EGF receptor modulates receptor downregulation and signaling. Cell. Signal. *20*, 2145–2155.

Liao, Y.C., Ruan, J.W., Lua, I., Li, M.H., Chen, W.L., Wang, J.R., Kao, R.H., and Chen, J.H. (2012). Overexpressed hPTTG1 promotes breast cancer cell invasion and metastasis by regulating GEF-H1/RhoA signalling. Oncogene *31*, 3086–3097.

Lozano, J., Xing, R., Cai, Z., Jensen, H.L., Trempus, C., Mark, W., Cannon, R., and Kolesnick, R. (2003). Deficiency of kinase suppressor of Ras1 prevents oncogenic ras signaling in mice. Cancer Res. *63*, 4232–4238.

Macara, I.G., Lounsbury, K.M., Richards, S.A., McKiernan, C., and Bar-Sagi, D. (1996). The Ras superfamily of GTPases. FASEB J. *10*, 625–630.

Malliri, A., van der Kammen, R.A., Clark, K., van der Valk, M., Michiels, F., and Collard, J.G. (2002). Mice deficient in the Rac activator Tiam1 are resistant to Ras-induced skin tumours. Nature *417*, 867–871.

Marcotte, R., Brown, K.R., Suarez, F., Sayad, A., Karamboulas, K., Krzyzanowski, P.M., Sircoulomb, F., Medrano, M., Fedyshyn, Y., Koh, J.L., et al. (2012). Essential gene profiles in breast, pancreatic, and ovarian cancer cells. Cancer Discov *2*, 172–189.

Meiri, D., Marshall, C.B., Greeve, M.A., Kim, B., Balan, M., Suarez, F., Bakal, C., Wu, C., Larose, J., Fine, N., et al. (2012). Mechanistic insight into the microtubule and actin cytoskeleton coupling through dynein-dependent RhoGEF inhibition. Mol. Cell *45*, 642–655.

Michaud, N.R., Therrien, M., Cacace, A., Edsall, L.C., Spiegel, S., Rubin, G.M., and Morrison, D.K. (1997). KSR stimulates Raf-1 activity in a kinase-independent manner. Proc. Natl. Acad. Sci. USA *94*, 12792–12796.

Mizuarai, S., Yamanaka, K., and Kotani, H. (2006). Mutant p53 induces the GEF-H1 oncogene, a guanine nucleotide exchange factor-H1 for RhoA, resulting in accelerated cell proliferation in tumor cells. Cancer Res. *66*, 6319–6326.

Moodie, S.A., Willumsen, B.M., Weber, M.J., and Wolfman, A. (1993). Complexes of Ras.GTP with Raf-1 and mitogen-activated protein kinase kinase. Science *260*, 1658–1661.

Morrison, D.K. (2001). KSR: a MAPK scaffold of the Ras pathway? J. Cell Sci. *114*, 1609–1612.

Mulcahy, H.E., Lyautey, J., Lederrey, C., qi Chen, X., Anker, P., Alstead, E.M., Ballinger, A., Farthing, M.J., and Stroun, M. (1998). A prospective study of K-ras mutations in the plasma of pancreatic cancer patients. Clin. Cancer Res. *4*, 271–275.

Nguyen, A., Burack, W.R., Stock, J.L., Kortum, R., Chaika, O.V., Afkarian, M., Muller, W.J., Murphy, K.M., Morrison, D.K., Lewis, R.E., et al. (2002). Kinase suppressor of Ras (KSR) is a scaffold which facilitates mitogen-activated protein kinase activation in vivo. Mol. Cell. Biol. *22*, 3035–3045.

Oliveira, C., Velho, S., Moutinho, C., Ferreira, A., Preto, A., Domingo, E., Capelinha, A.F., Duval, A., Hamelin, R., Machado, J.C., et al. (2007). KRAS and BRAF oncogenic mutations in MSS colorectal carcinoma progression. Oncogene *26*, 158–163.

Ory, S., Zhou, M., Conrads, T.P., Veenstra, T.D., and Morrison, D.K. (2003). Protein phosphatase 2A positively regulates Ras signaling by dephosphorylating KSR1 and Raf-1 on critical 14-3-3 binding sites. Curr. Biol. *13*, 1356–1364.

Owens, D.M., and Keyse, S.M. (2007). Differential regulation of MAP kinase signalling by dual-specificity protein phosphatases. Oncogene *26*, 3203–3213.

Philp, A.J., Campbell, I.G., Leet, C., Vincan, E., Rockman, S.P., Whitehead, R.H., Thomas, R.J., and Phillips, W.A. (2001). The phosphatidylinositol

3′-kinase p85alpha gene is an oncogene in human ovarian and colon tumors. Cancer Res. *61*, 7426–7429.

Porfiri, E., and McCormick, F. (1996). Regulation of epidermal growth factor receptor signaling by phosphorylation of the ras exchange factor hSOS1. J. Biol. Chem. *271*, 5871–5877.

Prendergast, G.C., Khosravi-Far, R., Solski, P.A., Kurzawa, H., Lebowitz, P.F., and Der, C.J. (1995). Critical role of Rho in cell transformation by oncogenic Ras. Oncogene *10*, 2289–2296.

Qiu, R.G., Chen, J., Kirn, D., McCormick, F., and Symons, M. (1995). An essential role for Rac in Ras transformation. Nature *374*, 457–459.

Razidlo, G.L., Kortum, R.L., Haferbier, J.L., and Lewis, R.E. (2004). Phosphorylation regulates KSR1 stability, ERK activation, and cell proliferation. J. Biol. Chem. *279*, 47808–47814.

Ren, Y., Li, R., Zheng, Y., and Busch, H. (1998). Cloning and characterization of GEF-H1, a microtubule-associated guanine nucleotide exchange factor for Rac and Rho GTPases. J. Biol. Chem. *273*, 34954–34960.

Ritt, D.A., Monson, D.M., Specht, S.I., and Morrison, D.K. (2010). Impact of feedback phosphorylation and Raf heterodimerization on normal and mutant B-Raf signaling. Mol. Cell. Biol. *30*, 806–819.

Sahai, E., Olson, M.F., and Marshall, C.J. (2001). Cross-talk between Ras and Rho signalling pathways in transformation favours proliferation and increased motility. EMBO J. *20*, 755–766.

Samuels, Y., and Velculescu, V.E. (2004). Oncogenic mutations of PIK3CA in human cancers. Cell Cycle *3*, 1221–1224.

Sandelin, A., Wasserman, W.W., and Lenhard, B. (2004). ConSite: web-based prediction of regulatory elements using cross-species comparison. Nucleic Acids Res. *32*, W249–W252.

Sieburth, D.S., Sundaram, M., Howard, R.M., and Han, M. (1999). A PP2A regulatory subunit positively regulates Ras-mediated signaling during Caenorhabditis elegans vulval induction. Genes Dev. *13*, 2562–2569.

Sjöblom, T., Jones, S., Wood, L.D., Parsons, D.W., Lin, J., Barber, T.D., Mandelker, D., Leary, R.J., Ptak, J., Silliman, N., et al. (2006). The consensus coding sequences of human breast and colorectal cancers. Science *314*, 268–274.

Smit, V.T., Boot, A.J., Smits, A.M., Fleuren, G.J., Cornelisse, C.J., and Bos, J.L. (1988). KRAS codon 12 mutations occur very frequently in pancreatic adenocarcinomas. Nucleic Acids Res. *16*, 7773–7782.

Smith, F.D., Langeberg, L.K., Cellurale, C., Pawson, T., Morrison, D.K., Davis, R.J., and Scott, J.D. (2010). AKAP-Lbc enhances cyclic AMP control of the ERK1/2 cascade. Nat. Cell Biol. *12*, 1242–1249.

Sundaram, M., and Han, M. (1995). The C. elegans ksr-1 gene encodes a novel Raf-related kinase involved in Ras-mediated signal transduction. Cell *83*, 889–901.

Therrien, M., Chang, H.C., Solomon, N.M., Karim, F.D., Wassarman, D.A., and Rubin, G.M. (1995). KSR, a novel protein kinase required for RAS signal transduction. Cell *83*, 879–888.

Therrien, M., Michaud, N.R., Rubin, G.M., and Morrison, D.K. (1996). KSR modulates signal propagation within the MAPK cascade. Genes Dev. *10*, 2684–2695.

Vojtek, A.B., Hollenberg, S.M., and Cooper, J.A. (1993). Mammalian Ras interacts directly with the serine/threonine kinase Raf. Cell *74*, 205–214.

Warne, P.H., Viciana, P.R., and Downward, J. (1993). Direct interaction of Ras and the amino-terminal region of Raf-1 in vitro. Nature *364*, 352–355.

Wassarman, D.A., Solomon, N.M., Chang, H.C., Karim, F.D., Therrien, M., and Rubin, G.M. (1996). Protein phosphatase 2A positively and negatively regulates Ras1-mediated photoreceptor development in Drosophila. Genes Dev. *10*, 272–278.

Whitehead, I., Kirk, H., Tognon, C., Trigo-Gonzalez, G., and Kay, R. (1995). Expression cloning of lfc, a novel oncogene with structural similarities to guanine nucleotide exchange factors and to the regulatory region of protein kinase C. J. Biol. Chem. *270*, 18388–18395.

Xiao, H., Zhang, Q., Shen, J., Bindokas, V., and Xing, H.R. (2010). Pharmacologic inactivation of kinase suppressor of Ras1 sensitizes epidermal growth factor receptor and oncogenic Ras-dependent tumors to ionizing radiation treatment. Mol. Cancer Ther. *9*, 2724–2736.

Zhang, Z., and Gerstein, M. (2003). Of mice and men: phylogenetic footprinting aids the discovery of regulatory elements. J. Biol. *2*, 11.

Zhang, X.F., Settleman, J., Kyriakis, J.M., Takeuchi-Suzuki, E., Elledge, S.J., Marshall, M.S., Bruder, J.T., Rapp, U.R., and Avruch, J. (1993). Normal and oncogenic p21ras proteins bind to the amino-terminal regulatory domain of c-Raf-1. Nature *364*, 308–313.

Cancer Cell, Volume *25*

Supplemental Information

The RhoGEF GEF-H1 Is Required for Oncogenic RAS Signaling via KSR-1

Jane Cullis, David Meiri, Maria Jose Sandi, Nikolina Radulovich, Oliver A. Kent, Mauricio Medrano, Daphna Mokady, Josee Normand, Jose Larose, Richard Marcotte, Christopher B. Marshall, Mitsuhiko Ikura, Troy Ketela, Jason Moffat, Benjamin G. Neel, Anne-Claude Gingras, Ming-Sound Tsao, and Robert Rottapel

Supplemetal Data

Table S1, related to Figure 1: Documented RAS pathway mutations and GEF-H1 essentiality in cell lines used in shRNA screen

Cell line	Type	*H*	*N*	*K*	*BRAF*	*PIK3CA*	*PTEN*	*GEF*	Reference
1. BT-20	Breast	WT	WT	WT	WT	P539R/H 1047R	+		Kozma et al., 1987, Hoeflich et al., 2009, Hollestelle et al., 2007
2. BT-474	Breast	WT	WT	WT	WT	K111N	+		Hoeflich et al., 2009, Hollestelle et al., 2007
3. BT-549	Breast	WT	WT	WT	WT	WT	null		Hoeflich et al., 2009, Hollestelle et al., 2007
4. CAL-51	Breast	WT	WT	WT	WT	E542K	+		Hoeflich et al., 2009
5. CAMA-1	Breast	WT	WT	WT	WT	WT	D92H		Hoeflich et al., 2009, Hollestelle et al., 2007
6. EFM-19	Breast	WT	WT	WT	WT	H1047L	+		Hoeflich et al., 2009
7. HCC1143	Breast	WT	WT	WT	WT	WT	+		Hoeflich et al., 2009
8. HCC1187	Breast	WT	WT	WT	WT	WT	+		Davies et al., 2012
9. HCC1395	Breast	WT	WT	WT	WT	WT	null		Hoeflich et al., 2009
10. HCC1419	Breast	WT	WT	WT	WT	WT	+		Hoeflich et al., 2009
11. HCC1428	Breast	WT	WT	WT	WT	WT	+		Hoeflich et al., 2009
12. HCC1500	Breast	WT	WT	WT	WT	WT	+		Hoeflich et al., 2009
13. HCC1806	Breast	WT	WT	WT	WT	WT	+		Hoeflich et al., 2009
14. HCC1937	Breast	WT	WT	WT	WT	WT	null		Hoeflich et al., 2009, Hollestelle et al., 2007
15. HCC1954	Breast	WT	WT	WT	WT	H1047L	+		Hoeflich et al., 2009
16. HCC38	Breast	WT	WT	WT	WT	WT	+		Hoeflich et al., 2009
17. Hs578T	Breast	G12 D	WT	WT	WT	WT	+	Y	Kraus et al., 1984, Hoeflich et al., 2009, Hollestelle et al., 2007
18. KPL-1	Breast	WT	WT	WT	WT	E545K	+		Hoeflich et al., 2009
19. MCF-7	Breast	WT	WT	WT	WT	E545K	+		Hoeflich et al., 2009, Hollestelle et al., 2007
20. MDA-MB-157	Breast	WT	WT	WT	WT	WT	+		Hollestelle et al., 2007
21. MDA-MB-231	Breast	WT	WT	G13D	G464V	WT	+		Kozma et al., 1987, Hoeflich et al., 2009, Hollestelle et al., 2007
22. MDA-MB-361	Breast	WT	WT	WT	WT	E545K/ K567R	+		Hoeflich et al., 2009, Hollestelle et al., 2007
23. MDA-MB-436	Breast	WT	WT	WT	WT	WT	null		Hoeflich et al., 2009, Hollestelle et al., 2007
24. MDA-MB-453	Breast	WT	WT	WT	WT	H1047R	E307 K		Hoeflich et al., 2009, Hollestelle et al., 2007
25. MDA-MB-468	Breast	WT	WT	WT	WT	WT	null		Hoeflich et al., 2009, Hollestelle et al., 2007
26. SK-BR-3	Breast	WT	WT	WT	WT	WT	+		Hoeflich et al., 2009, Hollestelle et al., 2007
27. SUM1315	Breast	WT	WT	WT	WT	WT	+	Y	Hoeflich et al., 2009
28. SW527	Breast	WT	WT	WT	WT	WT	+		Hoeflich et al., 2009
29. T-47D	Breast	WT	WT	WT	WT	H1047R	+		Hoeflich et al., 2009, Hollestelle et al., 2007
30. ZR-75-1	Breast	WT	WT	WT	I326T*	WT	null		Hoeflich et al., 2009, Hollestelle et al., 2007
31. HCT116	Colon	WT	WT	G13D	WT	H1047R	+	Y	COSMIC
32. HRE1	Lung							Y	
33. 609050M	Ovarian								

34. A2780	Ovarian	WT	WT	WT	G643G[#]				Estep et al., 2007, Holford et al., 1998
35. A2780_Cis	Ovarian	WT	WT	WT	G643G[#]				Estep et al., 2007, Holford et al., 1998
36. MM_OVCAR432_ Bast1	Ovarian	WT	WT	WT				Y	Patton et al., 1998
37. OV-1946	Ovarian			WT	WT				Ouellet et al., 2008
38. OV-90	Ovarian				N486-P490del /G643G[#]			Y	Estep et al., 2007
39. OVCA1369_TR	Ovarian			WT	WT				Letourneau et al., 2012
40. OVCA433_Bast	Ovarian	WT	WT	WT					Patton et al., 1998
41. OVCA5	Ovarian	WT	WT	G12V	WT	WT	+		Ikediobi et al., 2006
42. OVCA8	Ovarian	WT	WT	WT	WT	WT	+		Ikediobi et al., 2006
43. OVCAR-3	Ovarian	WT	WT	WT	WT	WT	+		Estep et al., 2007, Holford et al., 1998
44. SK-OV-3	Ovarian	WT	WT	WT	WT	H1047R	+	Y	Estep et al., 2007, Holford et al., 1998, Ikediobi et al., 2006
45. TOV-1946	Ovarian			WT	WT				Letourneau et al., 2012
46. TOV-2223G	Ovarian			WT	WT				Ouellet et al., 2008
47. TOV-3133G	Ovarian			WT	WT			Y	Letourneau et al., 2012
48. AsPC-1	Pancreas			G12D			null		COSMIC
49. BxPC3	Pancreas			WT			+		COSMIC
50. CFPAC-1	Pancreas			G12V			+	Y	COSMIC
51. Capan-2	Pancreas			G12V			+		COSMIC
52. HPAC	Pancreas			G12D			+		COSMIC
53. HPAF-II	Pancreas			G12D			null	*Y*	COSMIC
54. HPDE	Pancreas			WT			null		TRC
55. Hs_766T	Pancreas			WT	WT		null		COSMIC
56. IMIM-PC-1	Pancreas			G12D			null	Y	TRC
57. IMIM-PC-2	Pancreas			G12D			+		COSMIC
58. KP-3	Pancreas			G12V			null		TRC
59. KP-4	Pancreas			G12D			null		TRC
60. MiaPaCa-2	Pancreas			G12C			+		COSMIC
61. Panc 02.03	Pancreas			G12D			null	Y	TRC
62. Panc 03.27	Pancreas			G12V			+		TRC
63. Panc 04.03	Pancreas			G12D			+	*Y*	TRC
64. Panc 05.04	Pancreas			G12D			null		TRC
65. Panc 08.13	Pancreas			G12D			+	*Y*	TRC
66. Panc 10.05	Pancreas			G12D			+		TRC
67. PANC-1	Pancreas		WT	G12D	WT		+	*Y*	COSMIC
68. PaTu_8988S	Pancreas			G12V			null		TRC
69. PaTu_8988T	Pancreas			G12V			+	Y	TRC
70. PL45	Pancreas			G12D			+	*Y*	TRC
71. RWP-1	Pancreas			G12D			+	Y	TRC
72. SK-PC-1	Pancreas			G12D			+		COSMIC
73. SK-PC-3	Pancreas			G12V			+		TRC
74. SU.86.86	Pancreas			G12D			+		TRC
75. SW1990	Pancreas		WT	G12D	WT		+		COSMIC

H, HRAS; N, NRAS; K, KRAS; GEF, GEF-H1

Y, Important for survival/growth as identified in shRNA screen; *Y*, Important for survival/growth as identified and/or validated in *in vitro* studies

*, Functional effect of the listed mutation is unknown; #, Silent mutation

COSMIC, COSMIC database: http://cancer.sanger.ac.uk/cancergenome/projects/cosmic/

TRC, Mutation data obtained from The RNAi Consortium (TRC) group at the Donnelly Centre for Cellular and Biomolecular Research (University of Toronto, Toronto, Canada)
Blank cells, Information not found

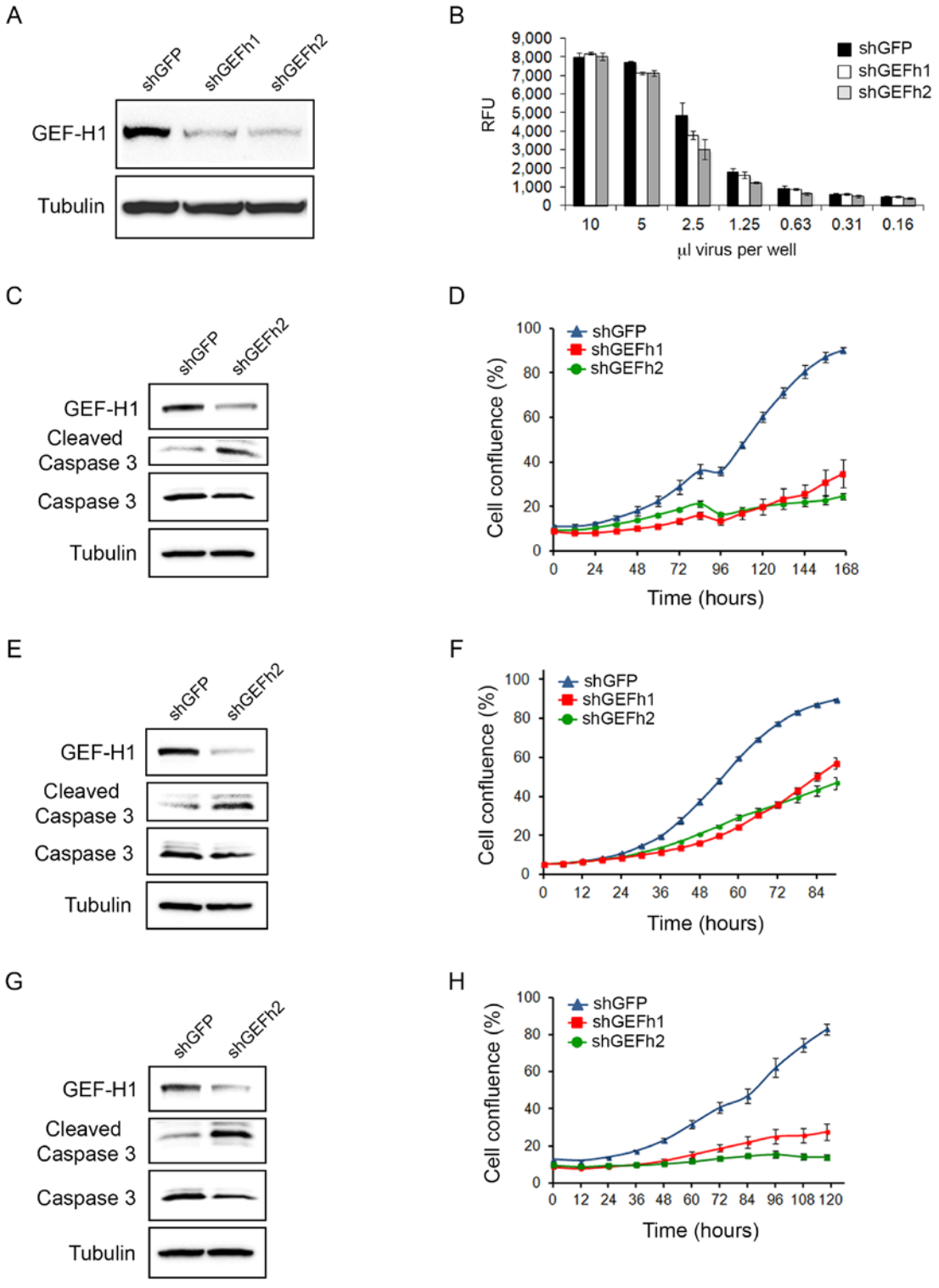

Figure S1, related to Figure 1. GEF-H1 contributes to the survival fitness of a subset of human cancer cell lines. (A) Western blot analysis of GEF-H1 expression in HEK 293T cells

stably expressing shGFP, shGEFh1 or shGEFh2. Tubulin served as a protein loading control. (B) Relative viral titering of shGFP, shGEFh1 and shGEFh2 lentivirus-infected HEK 293T cells measuring cell viability with decreasing volumes of virus (RFU= Relative Fluorescence Units). (C, E, G) Western blot analysis of caspase 3 cleavage following GEF-H1 protein depletion in OV-90 (C), HCT116 (E) and Panc 02.03 (G) cells 5 days after infection with shGFP or shGEFh2 lentivirus and selection with puromycin. Full length caspase 3 levels are shown and tubulin served as a protein loading control. (D, F, H) Growth curves of shGFP, shGEFh1 and shGEFh2-expressing OV-90 (D), HCT116 (F) and Panc 02.03 (H) cell lines. Cell lines expressing GEF-H1 hairpins exhibited a 66%, 50% and 70% reduction in cell growth relative to control hairpin-expressing OV-90, HCT116 and Panc 02.03 cells, respectively. Data are representative of three independent experiments +/- SEM.

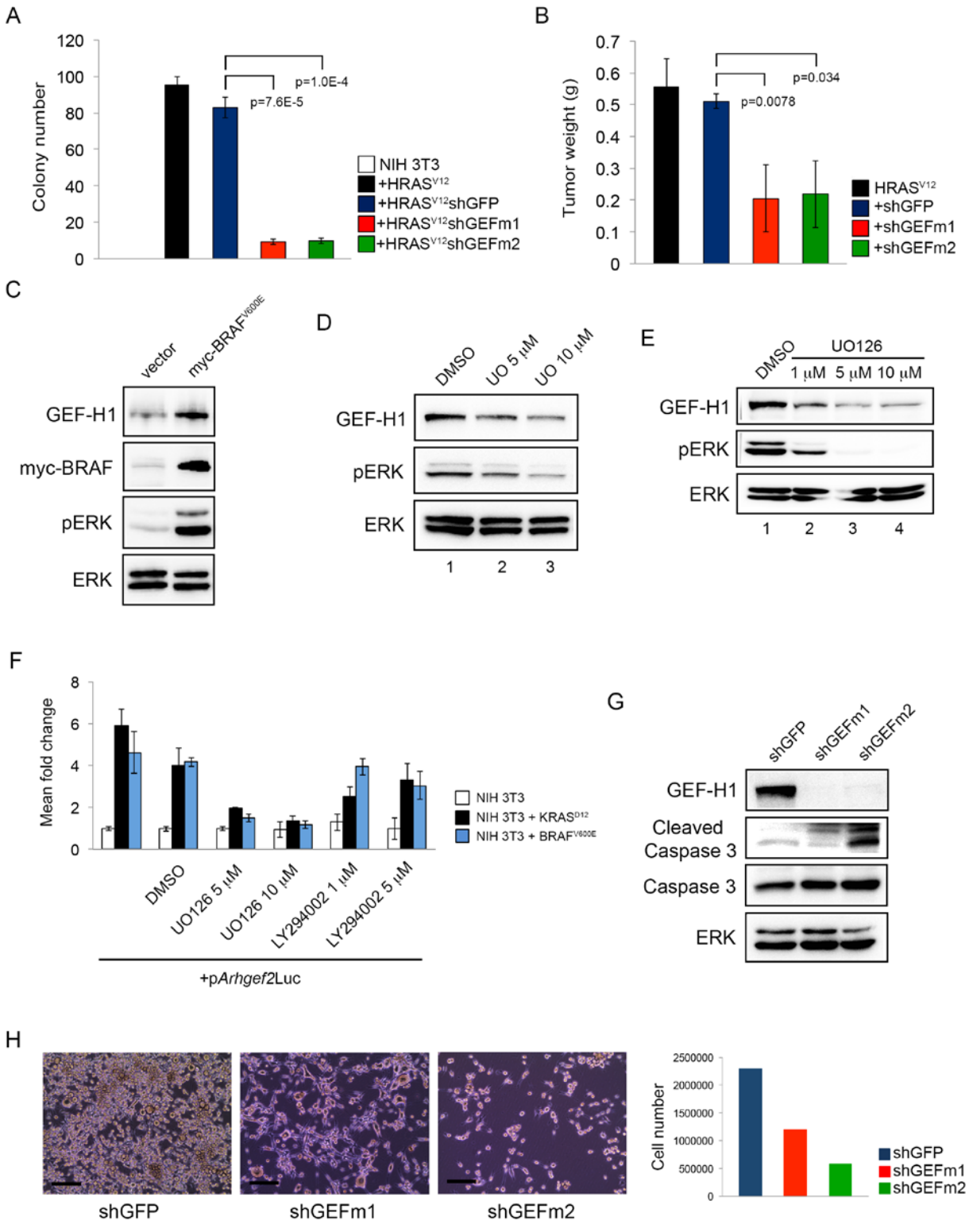
A
Colony number
120
100
80
60
40
20
0
p=1.0E-4
p=7.6E-5
NIH 3T3
+HRASV12
+HRASV12shGFP
+HRASV12shGEFm1
+HRASV12shGEFm2
B
Tumor weight (g)
0.7
0.6
0.5
0.4
0.3
0.2
0.1
0
p=0.034
p=0.0078
HRASV12
+shGFP
+shGEFm1
+shGEFm2
C
vector
myc-BRAFV600E
GEF-H1
myc-BRAF
pERK
ERK
D
DMSO
UO 5 μM
UO 10 μM
GEF-H1
pERK
ERK
1 2 3
E
DMSO
UO126
1 μM 5 μM 10 μM
GEF-H1
pERK
ERK
1 2 3 4
F
Mean fold change
8
6
4
2
0
NIH 3T3
NIH 3T3 + KRASD12
NIH 3T3 + BRAFV600E
DMSO
UO126 5 μM
UO126 10 μM
LY294002 1 μM
LY294002 5 μM
+pArhgef2Luc
G
shGFP
shGEFm1
shGEFm2
GEF-H1
Cleaved Caspase 3
Caspase 3
ERK
H
shGFP
shGEFm1
shGEFm2
Cell number
2500000
2000000
1500000
1000000
500000
0
shGFP
shGEFm1
shGEFm2

Figure S2, related to Figure 3. GEF-H1 contributes to cell survival and growth in HRAS^{V12}-and BRAF^{V600E}-transformed cells. (A) Quantification of colonies depicted in Figure 3C with greater than 2 mm in diameter in NIH 3T3 (n = 0), NIH 3T3-HRAS^{V12} (n = 95), NIH 3T3-HRAS^{V12}shGFP (n = 82), NIH 3T3-HRAS^{V12}shGEFm1 (n = 9) and NIH 3T3-HRAS^{V12}shGEFm2 (n = 9) cells. n denotes mean number of colonies per 60 mm dish with $1x10^3$ cells resuspended per dish per assay. Results are the combination of three independent experiments +/- SEM. (B) Final mean tumor weights of tumor xenografts shown in Figure 3D. Results are the combination of four independent experiments and a total of n=21 tumors per condition, with error bars indicating +/- SEM. (C) Western blot showing GEF-H1 expression in NIH 3T3 cells stably expressing empty vector or myc-BRAF^{V600E}. pERK levels indicate level of MAPK activation and total ERK levels served as a protein loading control. (D) Western blot of GEF-H1 expression in stable myc-BRAF^{V600E}-expressing NIH 3T3 cells treated with DMSO (lane 1), or increasing concentrations of the MEK inhibitor UO126 (lanes 2 and 3) for 48 hr. pERK levels show degree of MAPK pathway inhibition and total ERK served as a protein loading control. (E) A375 human melanoma cells harboring an endogenous *BRAF^{V600E}* mutation were treated with DMSO (lane 1) or increasing concentrations of UO126 (lanes 2-4) for 48 hr. GEF-H1 levels were assessed by probing whole cell lysates with anti-GEF-H1 antibodies. pERK levels reflect degree of MAPK inhibition and total ERK served as a protein loading control. (F) *Arhgef2* promoter activity in NIH 3T3 cells expressing empty vector, KRAS^{D12} or BRAF^{V600E} and transfected with a pGL3 luciferase expression vector driven by the murine *Arhgef2* promoter region (p*Arhgef2*Luc). p*Arhgef2*Luc-expressing cells were treated with DMSO or indicated concentrations of UO126 and LY294002 for 16 hr. Luciferase activity was measured 24 hr after transfection, normalized to renilla expression and is represented as fold change over empty

vector-expressing NIH 3T3 cells. Data are representative of three independent experiments +/- SEM. (G) Western blot analysis of caspase 3 cleavage following stable depletion of GEF-H1 protein levels in NIH 3T3-BRAF^{V600E} cells. Full-length caspase 3 levels are shown and tubulin served as a protein loading control. (H) Bright field images (left) and quantification of cell numbers (right) in NIH 3T3-BRAF^{V600E} cells infected with shGFP, shGEFm1 or shGEFm2 five days after infection. Scale bars represent 100 μm.

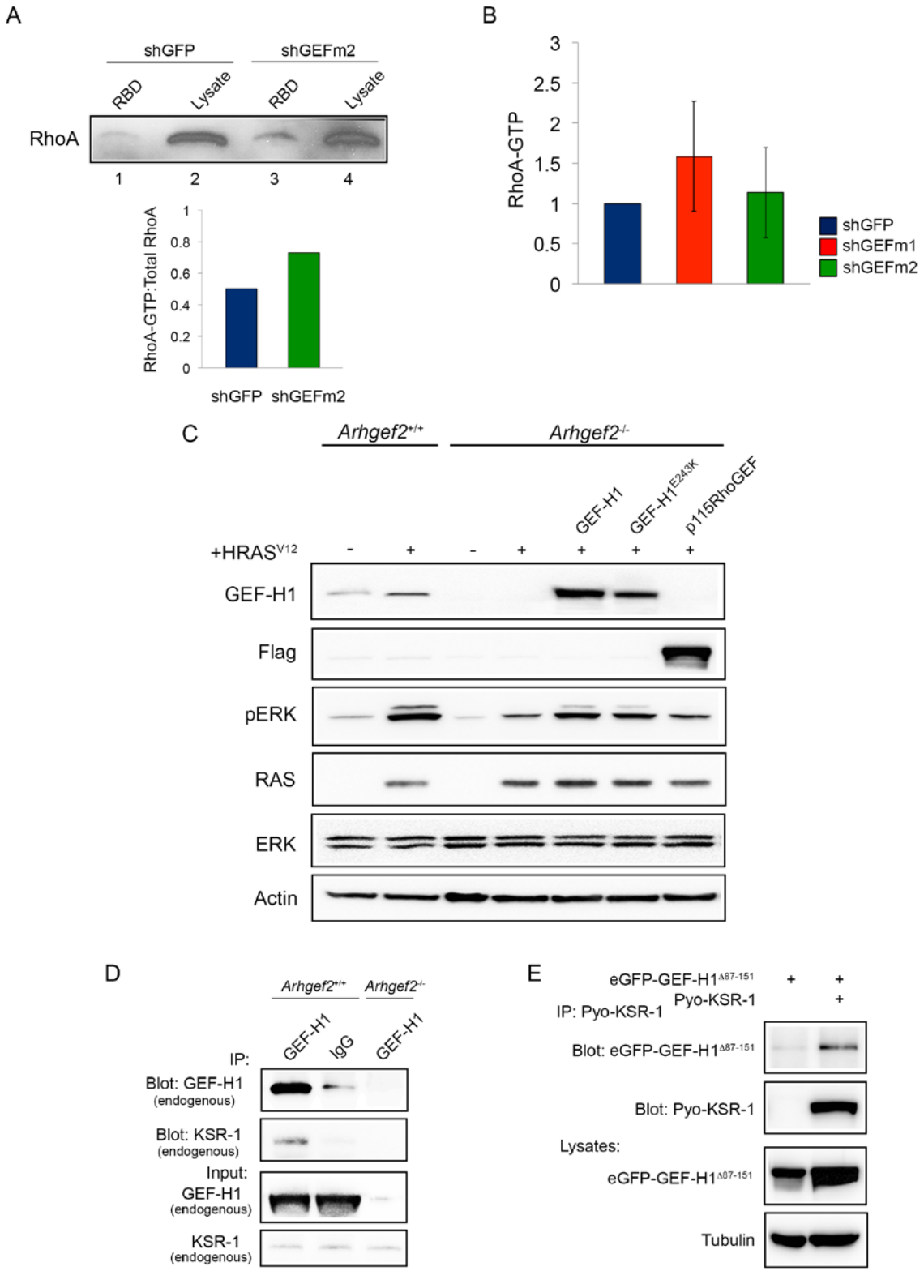
A
shGFP
shGEFm2
RBD
Lysate
RBD
Lysate
RhoA
1
2
3
4
RhoA-GTP:Total RhoA
shGFP
shGEFm2
B
RhoA-GTP
shGFP
shGEFm1
shGEFm2
C
Arhgef2+/+
Arhgef2-/-
GEF-H1
GEF-H1E243K
p115RhoGEF
+HRASV12
GEF-H1
Flag
pERK
RAS
ERK
Actin
D
Arhgef2+/+
Arhgef2-/-
IP:
GEF-H1
IgG
GEF-H1
Blot: GEF-H1 (endogenous)
Blot: KSR-1 (endogenous)
Input: GEF-H1 (endogenous)
KSR-1 (endogenous)
E
eGFP-GEF-H1Δ87-151
Pyo-KSR-1
IP: Pyo-KSR-1
Blot: eGFP-GEF-H1Δ87-151
Blot: Pyo-KSR-1
Lysates:
eGFP-GEF-H1Δ87-151
Tubulin

Figure S3, related to Figure 4. GEF-H1 is necessary for optimal MAPK activation in HRAS^{V12}-transformed cells. (A) Lysates derived from HRAS^{V12}-transformed NIH 3T3 cells stably expressing control hairpin (shGFP) or murine GEF-H1 shRNA (shGEFm2) were incubated with GST-tagged Rhotekin-Rho binding domain (GST-RBD). Active RhoA-GTP in GST-RBD pulldowns (lanes 1 and 3) and total cellular RhoA (lanes 2 and 4) were detected by immunoblotting with anti-RhoA antibody. Normalization of RhoA-GTP to total cellular RhoA for each experimental condition is shown graphically below. (B) RhoA-GTP levels in serum-starved shGFP, shGEFm1 and shGEFm2 cells expressing HRAS^{V12} as quantified by RhoA G LISA. Data are representative of three independent experiments +/- SEM. (C) *Arhgef2*$^{+/+}$ or *Arhgef2*$^{-/-}$ MEFs were transfected with eGFP, eGFP-HRAS^{V12} or co-transfected with eGFP-HRAS^{V12} and Flag-GEF-H1, eGFP-HRAS^{V12} and Flag-GEF-H1^{E243K} or eGFP-HRAS^{V12} and Flag-p115RhoGEF and assayed for pERK by western blot. Blots were probed with anti-GEF-H1, anti-Flag and anti-RAS antibodies to confirm the expression of transfected plasmids. Actin served as a protein loading control. (D) Wild-type or *Arhgef2*$^{-/-}$ MEFs were immunoprecipitated with anti-GEF-H1 antibodies or control IgG and probed for the presence of endogenous KSR-1. Total protein levels of GEF-H1 and KSR-1 are shown in lower panel. (E) HEK 293T cells were transfected with eGFP-GEF-H1$^{\Delta 87\text{-}151}$ or eGFP-GEF-H1$^{\Delta 87\text{-}151}$ and Pyo-KSR-1 and Pyo-KSR-1 immunoprecipitates were probed for the presence of eGFP-GEF-H1$^{\Delta 87\text{-}151}$. Total levels of eGFP-GEF-H1$^{\Delta 87\text{-}151}$ are shown and tubulin served as a loading control.

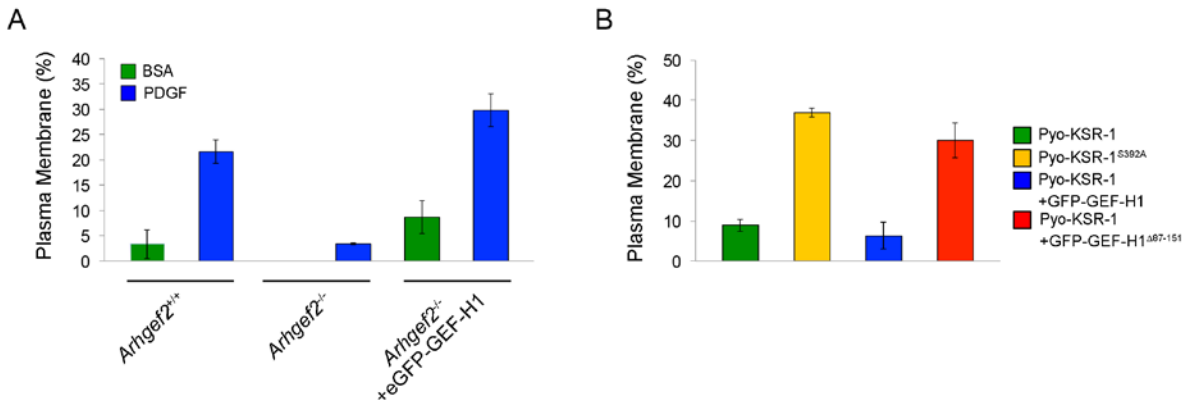

Figure S4, related to Figure 5. GEF-H1 is required for PDGF-induced plasma membrane translocation of KSR-1. (A) Percentage of cells described in Figure 5A exhibiting KSR-1 plasma membrane translocation. (B) Percentage of cells described in Figure 5B exhibiting KSR-1 translocation. At least 60 cells were imaged per condition and all data are the mean of three independent experiments +/- SD.

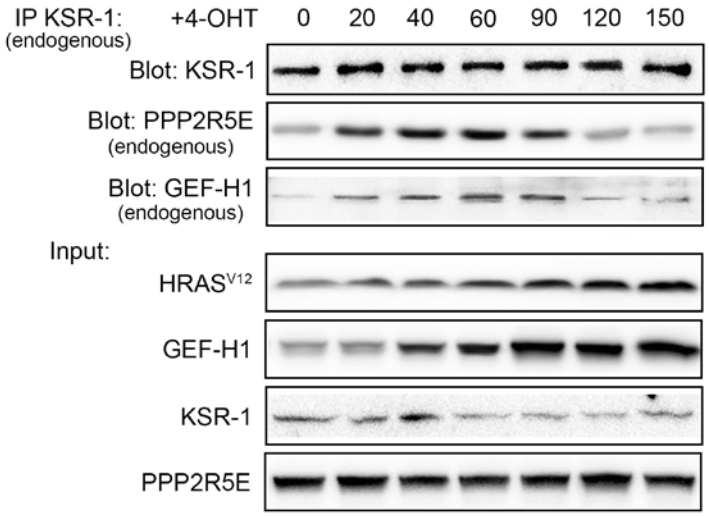

Figure S5, related to Figure 6. Endogenous KSR-1:GEF-H1:PPP2R5E complex formation is induced by oncogenic HRAS. Endogenous KSR-1 was immunoprecipitated from ER:HRAS^{V12} MEFs at 0, 30, 60, 90, 120 and 150 min following acute induction of HRAS^{V12} with 100 nM 4-OHT. KSR-1 immune complexes were probed for the presence of endogenous PPP2R5E and GEF-H1. Total cellular levels of ER:HRAS^{V12}, GEF-H1, KSR-1 and PPP2R5E are shown in the lower panel.

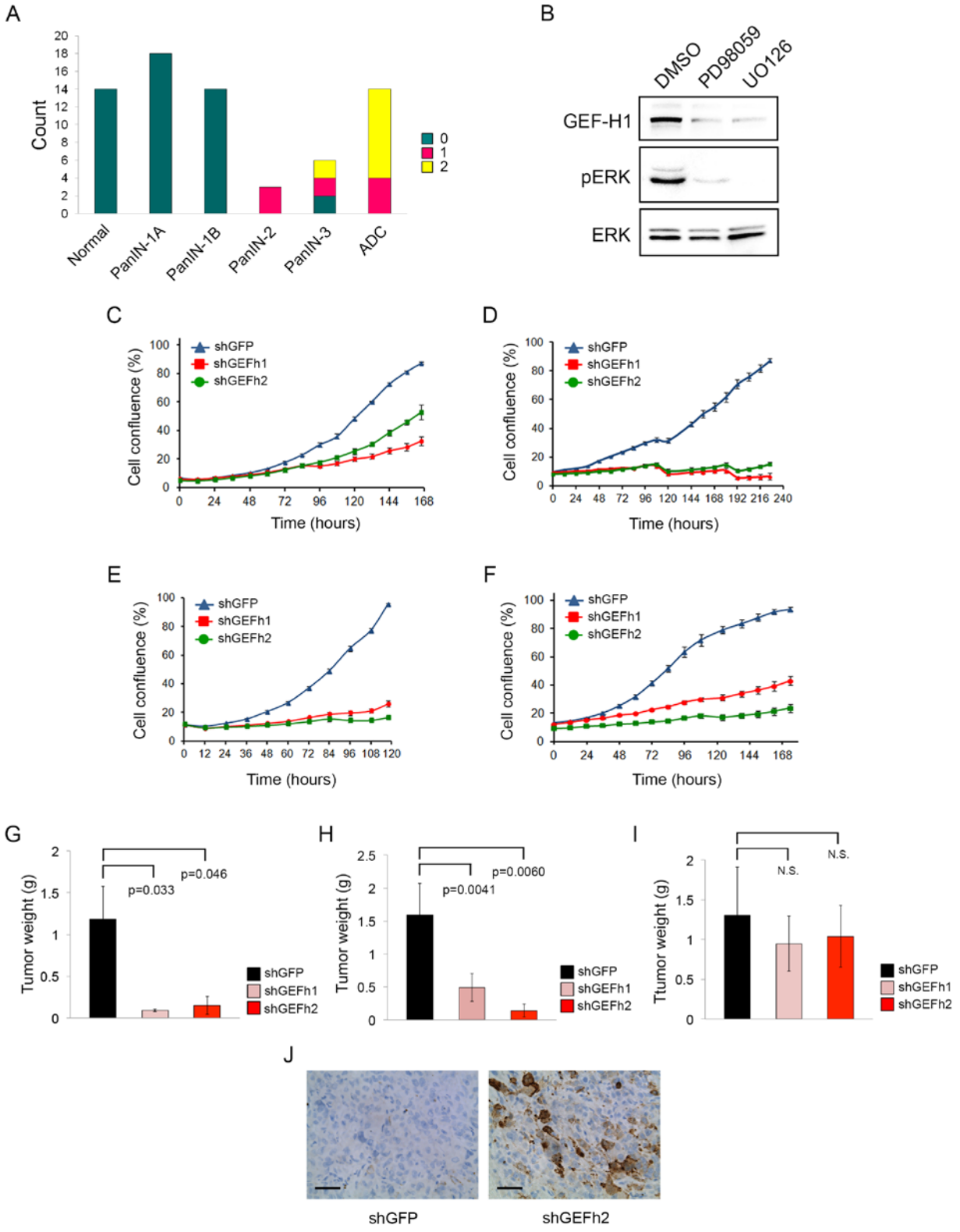
A
Count
Normal
PanIN-1A
PanIN-1B
PanIN-2
PanIN-3
ADC
0
1
2
B
DMSO
PD98059
UO126
GEF-H1
pERK
ERK
C
Cell confluence (%)
Time (hours)
shGFP
shGEFh1
shGEFh2
D
Cell confluence (%)
Time (hours)
shGFP
shGEFh1
shGEFh2
E
Cell confluence (%)
Time (hours)
shGFP
shGEFh1
shGEFh2
F
Cell confluence (%)
Time (hours)
shGFP
shGEFh1
shGEFh2
G
Tumor weight (g)
p=0.033
p=0.046
shGFP
shGEFh1
shGEFh2
H
Tumor weight (g)
p=0.0041
p=0.0060
shGFP
shGEFh1
shGEFh2
I
Ttumor weight (g)
N.S.
N.S.
shGFP
shGEFh1
shGEFh2
J
shGFP
shGEFh2

Figure S6, related to Figure 7. GEF-H1 is important for RAS-mutant pancreatic tumor xenograft growth *in vitro* and *in vivo*. (A) Distribution of GEF-H1 immunoscores in Tissue Microarrays (TMAs) containing 14 normal, 32 PanIN-1A and PanIN-1B, 9 PanIN-2 and PanIN-3 and 9 ADC depicted in Figure 7A. Intensity in the ductal cells or lesions was scored as 0 (absent), 1 (weak) or 2 (strong). (B) PANC-1 cells were treated with DMSO, UO126 or PD98059 for 48 hr and GEF-H1 protein expression was assayed by western blot. pERK levels indicate degree of MEK inhibition and ERK served as a protein loading control. (C-F) Growth curves of shGFP, shGEFh1 and shGEFh2-expressing PANC-1 (C), Panc 08.13 (D), Panc 04.03 (E) and PL-45 (F) cells. GEF-H1 depletion resulted in a 50%, 90%, 80% and 65% reduction in cell growth compared to hairpin controls for each cell line, respectively. Data are representative of three independent experiments +/- SEM. (G-I) Mean final tumor weights of PANC-1 (G), HPAF-II (H) and BxPC3 (I) xenografts described in Figure 7C. Error bars represent +/- SD of one experiment from n=5 tumors and are representative of two independent experiments. (J) Representative images of xenografts derived from shGFP and shGEFh2-expressing PANC-1 (n=5 per condition) cells probed for cleaved caspase 3 by immunohistochemistry. Cleaved caspase 3 expression is depicted in brown. Scale bars represent 100 μm.

Supplemental Experimental Procedures

shRNA screen. The genome-wide pooled shRNA screen was performed as described in Marcotte et al., 2012. Briefly, 75 tumor-derived cell lines (30 breast, 1 colorectal, 1 lung, 15 ovarian and 28 pancreatic) were infected with a library of 78, 432 small hairpin RNAs targeting 16, 056 unique Refseq genes (yielding an average of 5 shRNAs targeting each gene) developed by The RNAi Consortium (TRC). Each cell line was screened in triplicate and at least 3 time points were assessed for overall shRNA abundance during population outgrowth. shRNA Activity Ranking Profiles ('shARP') scores were assigned to each hairpin by calculating the average slope between the microarray intensity at each time point and time zero. To determine the behavior of specific genes, the Gene Activity Ranking Profile (GARP) score was calculated as the average of the two lowest shARP scores. See Table S1 for RAS/BRAF pathway mutation status and *ARHGEF2* essentiality in each cell line.

Cell lines and cell culture. All cultures were maintained in a 5% CO_2 environment at 37^{o}C. NIH 3T3 (ATCC), MEFs, ER:HRAS^{V12} MEFs (Julian Downward, London Research Institute, London, UK), HEK 293T (ATCC), NIH 3T3-KRAS^{D12} (NIH), A375 (Benjamin Neel, Ontario Cancer Institute, Toronto, ON), PANC-1 (ATCC), HPAF-II (ATCC), and PL-45 (ATCC) cell lines were cultured in DMEM (Life Technologies Inc.) supplemented with 10% fetal bovine serum (FBS) (HyClone). BxPC3 (ATCC) cells were cultured in RPMI 1640 (Life Technologies, Inc.) supplemented with 10% FBS. Panc 02.03, Panc 04.03 and Panc 08.13 (Troy Ketela, Donnelly Centre and Banting & Best Department of Medical Research, Toronto, ON) cells were cultured in RPMI 1640 supplemented with 10 units/ml human insulin (Wisent BioProducts, Inc.) and 15% FBS. HCT116 (ATCC) cells were maintained in McCoy's 5A Modified Medium (Life Technologies Inc.) supplemented with 10% FBS. OV-90 cells (ATCC) were cultured in OSE

medium (Wisent 316-030CL) supplemented with 10% FBS and G418 (Sigma, 400μg/ml). MEFs and NIH 3T3/HEK 293T cells were transfected using Effectene (QIAGEN) and Polyfect (QIAGEN), respectively, according to manufacturer's instructions. Stable $HRAS^{V12}$, $KRAS^{D12}$ and $NRAS^{D12}$-expressing NIH 3T3 cells were established by selecting transfected cells with 400μg/mL G418 (Sigma). Stable NIH 3T3-$BRAF^{V600E}$-expressing cells were established by infecting NIH 3T3 cells with myc-$BRAF^{V600E}$ retrovirus and selecting for infected cells with 1.5 μg/ml puromycin (Sigma) for 72 hr. *Arhgef2*$^{-/-}$ MEFs were generated as described previously (Meiri et al., 2012) and maintained in DMEM + 10% FBS. *Ksr-1*$^{-/-}$ MEFs were kindly given to us by D. Morrison (National Cancer Institute, Frederick, MD) and maintained in DMEM + 10% FBS. PP2A subunit-expressing HEK 293T cells were graciously provided by A.C. Gingras (Samuel Lunenfeld Research Institute, Toronto, ON) and were maintained in DMEM + 10% FBS. Stable murine and human GEF-H1 knockdown cell lines were established by co-transfecting HEK 293T cells with lentiviral hairpin plasmids targeting murine or human *ARHGEF2* with packaging plasmids pPAX2 and VSV-g using the CalPhos Mammalian Transfection Kit (Clontech). After 48 hr lentiviral supernatants were collected, filtered through a 0.45 μm PVDF membrane and incubated with target cells in the presence of 7 μg/ml Polybrene (Sigma). 48 hr after infection target cells were selected with 2-5 μg/ml puromycin until all untransduced cells died.

Caspase 3 cleavage. NIH 3T3-$HRAS^{V12}$ and NIH 3T3-$BRAF^{V600E}$ cells were infected with shGFP, shGEFm1 or shGEFm2 lentivirus and OV-90, HCT116 and Panc 02.03 cells were infected with shGFP or shGEFh2 lentivirus. After 24 hr cells were placed in 2-4 μg/ml puromycin selection medium for 72 hr. 24 hr following selection cells were lysed in 2X sample

buffer, boiled, sonicated and resolved by SDS-PAGE and transfer to PVDF membranes for immunoblotting using anti-GEF-H1, anti-caspase 3 (CST #9665) and anti-tubulin antibodies.

Viral titering. Relative viral titering was performed according to the Resazurin (alamarBlueR) Cell Viability Assay obtained from The RNAi Consortium (TRC, http://www.broadinstitute.org). Briefly, highly infectable HEK 293T cells were plated in 96-well plates at 5-10x10^3 cells per well and infected with decreasing volumes of virus for 24 hr. Cells were then selected with puromycin for 48 hr and cell viability was assayed with alamarBlue® according to manufacturer's protocol. Relative viral titering was performed in triplicate for each condition and values are representative of three independent experiments.

Expression constructs. Full-length, truncated and mutated GEF-H1 constructs (accession no. AF177032 (mouse) and NM_004723.3 (human) were cloned into the pFlag-CMV2 vector (Sigma) or pEGFP-C1 (Invitrogen). Murine p115 RhoGEF cDNA (accession no. NM_001130150.1) was cloned into pFlag-CMV2 vector. Murine *Arhgef2* pLKO.1 lentiviral shRNA and shGFP constructs were obtained from The RNAi Consortium (TRC) and human *ARHGEF2* shRNA sequences were cloned into the EcoRI and AgeI restriction sites of pLKO.1 (sequences denoted below). pCGT-H-, K-, $NRAS^{V/D12}$ and pCMV-Flag-AKAPLbc constructs were kind gifts from D. Bar Sagi (Langone Medical Centre, New York, NY) and J. Scott (Howard Hughes Medical Institute, Seattle, WA), respectively. pBABE-puro-$BRAF^{V600E}$ retrovirus was obtained from Addgene. pCDNA3-Pyo-KSR-1 wild-type, mutant and truncated expression vectors were kind gifts from D. Morrison (Centre for Cancer Research, Frederick, MD, described in Muller et al., 2001).

Murine and human *ARHGEF2* shRNA sequences:

Arhgef2 shRNA 1 (shGEFm1)

F: 5'-CCGGGCAGGAGATTTACAACCGAATCTCGAGATTCGGTTGTAAATCTCCTGTTTTTG-3'

R: 5'-AATTCAAAAAGCAGGAGATTTACAACCGAATCTCGAGATTCGGTTGTAAATCTCCTGTT-3'

Arhgef2 shRNA 2 (shGEFm2)

F: 5'-CCGGCCCTCATTTGTCCTACATGTACTCGAGTACATGTAGGACAAATGAGGGTTTTTG-3'

R: 5'-AATTCAAAAACCCTCATTTGTCCTACATGTACTCGAGTACATGTAGGACAAATGAGGGTT-3'

ARHGEF2 shRNA 1 (shGEFh1)

F: 5'-CCGGAACCACGGAACTGGCATTACTCTCGAGAGTAATGCCAGTTCCGTGGTTTTTTTG-3'

R: 5'-AATTCAAAAAAACCACGGAACTGGCATTACTCTCGAGAGTAATGCCAGTTCCGTGGTT-3'

ARHGEF2 shRNA 2 (shGEFh2)

F: 5'-CCGGAATGTGACTATCCACAACCGCCTCGAGGCGGTTGTGGATAGTCACATTTTTTTG-3'

R: 5'-AATTCAAAAAAATGTGACTATCCACAACCGCCTCGAGGCGGTTGTGGATAGTCACATT-3'

GFP shRNA (shGFP)

F: 5'-CCGGTGCCCGACAACCACTACCTGACTCGAGTCAGGTAGTGGTTGTCGGGCA TTTTTG-3'

R: 5'-AATTCAAAAATGCCCGACAACCACTACCTGACTCGAGTCAGGTAGTGGTTGTCGGGCA-3'

Immunoprecipitation and western blot. For immunoprecipitation experiments, cells were scraped into ice cold lysis buffer (30 mM Tris pH 7.5, 150 mM NaCl, 1% Triton X-100, 0.2% sodium deoxycholate, 10 mM NaF, 1 mM Na_3VO_4 and 1 mM PMSF) with Complete Protease Inhibitor cocktail (Roche) and cleared extracts incubated with protein G sepharose and appropriate antibodies for 2 hr at 4^0C. Immunoprecipitates were washed three times with wash buffer (30 mM Tris pH 7.5, 300 mM NaCl, 5 mM NaF and 0.1% Triton X-100), resuspended in 2X sample buffer, boiled and protein complexes resolved by SDS-PAGE before transfer to PVDF (Imobilon) membranes and immunoblotting. For western blotting, cells were scraped into ice cold lysis buffer described above and incubated on ice for 20 min, followed by centrifugation at 16, 060 xg at 4^oC for 10 min. Cleared lysates were resuspended in 2X sample buffer, boiled for 5 min and protein resolved by SDS-PAGE before transfer to PVDF membranes and immunoblotting. Alternately, cells were lysed directly in 2X sample buffer and boiled for 5 min before being resolved by SDS-PAGE.

Antibodies. Polyclonal sheep anti-GEF-H1 (recognizing murine and human GEF-H1) antibodies were raised as described previously (Bakal et al., 2005). Monoclonal mouse anti-GEF-H1 human antibodies 3C5 and 14B11 were designed using N- and C-terminal human GEF-H1 peptides and produced by hybridoma. Western blotting and immunofluorescence were performed using the following primary antibodies: anti-RAS (CST, 3965), anti-p44/42 MAPK (ERK1/2) (CST, 9102), anti-phospho-p44/42 MAPK (ERK1/2) Thr202/Tyr204 (CST, 9106), anti-MEK1/2 (CST, 9122), anti-phospho-MEK1/2 Ser217/221 (CST, 9154), anti-caspase 3 (CST, 9665), anti-cleaved caspase 3 (CST, 9661), anti-KSR-1 (gift from D. Morrison, see Cacace et al., 1999), anti-phospho-KSR-1 S392 (CST, 2502), anti-PP2Ac (Millipore, 05-421), anti-RhoA (CST, 2117), anti-alpha tubulin (Molecular Probes), anti-Flag (M2, F3165, Sigma), anti-GFP (Invitrogen, G10362), anti-myc (Sigma, M4439) and anti-Pyo (CST, 2448s). HRP-conjugated anti-mouse or anti-rabbit secondary antibodies were from GE Healthcare.

Quantitative PCR. RNA was extracted from NIH 3T3 or NIH 3T3-HRAS^{V12} cell lines using the RNeasy mini kit (QIAGEN). 100 ng of RNA was converted into double-stranded cDNA at 42^{o}C with SuperScript II RNase H-reverse transcription kit (Invitrogen). qPCR was performed with 50 ng of template cDNA mixture from each cell line and mouse Taqman gene expression assays for *Arhgef2* (Mm00434757_m1, Applied Biosystems) and *Tubulin* (Mm00846967_g1, Applied Biosystems). Gene expression levels in the samples were calculated relative to control using the comparative C_T method: $\Delta\Delta C_T = \Delta C_{Tsample} - \Delta C_{Tcontrol}$, fold change = $2^{-\Delta\Delta CT}$. Tubulin expression was used to normalize target gene expression levels.

RBD pulldown assay and RhoA G LISA. For pulldown experiments active RhoA was assessed by incubation of cell lysates with GST-Rhotekin-RBD (Cytoskeleton, CO, USA). Sub-confluent NIH 3T3-HRAS^{V12} cells stably expressing shGFP or shGEFm2 were serum-starved for 16 hr and

lysed in ice cold HNMETG lysis buffer (50 mM HEPES pH 7.5, 150 mM NaCl, 1.5 mM $MgCl_2$, 1 mM EGTA, 1% Triton-X 100 and 10% glycerol). Lysates were clarified by centrifugation at 16, 060xg at 4^{o}C, equalized for total volume loading and rotated for 60 min at 4^{o}C with 20 μg of purified GST-RBD bound to glutathione Sepharose beads. The beads were washed three times with HNMETG wash buffer (50 mM HEPES pH 7.5, 300 mM NaCl, 1.5 mM $MgCl_2$, 1 mM EGTA, 0.1% Triton-X 100 and 10% glycerol) and processed for SDS-PAGE. For RhoA-GTP quantitation using RhoA G LISA kit (Cytoskeleton, CO, USA), sub-confluent NIH 3T3-$HRAS^{V12}$ cells stably expressing shGFP, shGEFm1 or shGEFm2 were serum-starved for 16 hr, washed, lysed in ice cold lysis buffer, cleared, snap-frozen in liquid nitrogen and stored at -70^{o}C. Equal levels of total RhoA was confirmed with the Precision Red Advanced Protein Assay Reagent (Cytoskeleton) and lysates were processed for RhoA-GTP quantitation according to manufacturer's protocol. Total GTP-bound RhoA was determined from cell lysates in triplicate and mean values from two independent experiments are shown +/- SD.

NMR-based GEF assay. To measure GEF activity in lysates of mammalian cells, NMR was performed as described in Marshall et al., 2012. To measure RhoA activity of wild-type eGFP-GEF-H1, eGFP-GEF-$H1^{\Delta 87\text{-}151}$ eGFP-GEF-$H1^{E243K}$ and eGFP-p115RhoGEF, plasmids were transfected into HEK 293T cells using Polyfect (QIAGEN) and NMR analysis was performed on lysates as described previously.

Anchorage-independent growth. 60 mm dishes were coated with bottom agar consisting of 0.6% ultra-pure agarose (Sigma), 2X DMEM and 25% FBS and allowed to solidify at 4^{0}C for 30 min. 1x10^4 cells were resuspended in top agar consisting of 0.4% agarose, 2X DMEM and 25% FBS at 37^{0}C and poured over bottom agar. Growth medium was refreshed every 3 days. After 10 days dishes were stained with 1 ml of 0.0005% crystal violet in 70% ethanol for 4 hr at room

temperature and imaged at 10X or 40X on a dissecting microscope. Colonies greater than 2 mm in diameter were counted manually at 10X magnification in triplicate. Results represent the mean of 3 independent experiments +/- SE.

Cell growth assays. OV-90, HCT116, Panc 02.03, PANC-1, Panc 08.13, Panc 04.03 and PL-45 cells were plated in 12-well plates at $1x10^5$-$1.5x10^5$ cells per well. After 24 hr cells were infected with a multiplicity of infection (MOI) of 5 of shGFP, shGEFh1 or shGEFh2 lentivirus for 24 hr. Hairpin-expressing cells were selected with 3-5 μg/ml puromycin for 48 hr. Selected cells were then re-plated in 96-well plates at $5x10^3$ cells per well in quadruplicate in regular growth medium and placed directly into the INCUCYTE^{TM} Kinetic Imaging System (Essen Bioscience) to monitor cell growth. Cells were re-fed every 3-4 days with medium containing puromycin and percent cell confluence was monitored until shGFP-expressing cells reached confluence. Values represent the mean of three independent experiments +/- SEM.

Immunofluorescence imaging. Cells grown on glass coverslips were treated as indicated in the corresponding figure legends and fixed with 4% PFA for 10 min, washed three times with 1X PBS and permeabilized with 0.1% Triton X-100 for 5 min. The coverslips were blocked with 0.5% w/v bovine serum albumin (BSA) in 1X PBS for 1 hr at room temperature and incubated with primary antibody (α-KSR-1 1:200) in 0.5% BSA/1X PBS at 37^{o}C for 30 min or at 4^{o}C overnight. Coverslips were washed three times with 1X PBS and incubated with secondary antibody (red anti-mouse 1:400) at 37^{o}C for 1 hr. Slides were mounted using GelTol mounting medium (Shandon Immunon, Thermo Electron Corporation). Confocal imaging was performed with an Olympus IX81 inverted microscope using a 60X zoom x3 (1.4 NA; PlanApo, Nikon) objective, and FluoView software (Olympus, Tokyo, Japan). Resolution was 512 x 512 with 12 bits/pixel. The following excitation wavelengths were used for GFP (473 nm) and Texas Red

(559 nm). All images in each set of experiments were acquired with the same microscope sensitivity settings. All images compared within each figure panel were acquired on the same day, with identical staining conditions, gain and contrast setting, and same magnification. All statistical analyses were derived from 60 or more images from three independent experiments for each treatment condition.

Animal studies. Xenograft studies in nude mice with NIH 3T3 cell lines were performed using 8-week old athymic NCr nude mice (Taconic Laboratories, Hudson, NY). Mice were allowed to acclimatize for one week before being injected subcutaneously in the hip flank with $1x10^6$ cells resuspended in 40 μl of 1:1 phosphate-buffered saline (PBS, Life Technologies) and growth factor-reduced matrigel (BD Biosciences). Mice were housed 3-4 to a cage and tumors were allowed to grow until they reached a maximum of 1.5 cm in diameter or became ulcerated, at which point mice were sacrificed by carbon dioxide asphyxiation. Tumors were removed, weighed, measured and fixed in OCT medium for histologic processing. Five injections were performed per condition over four independent experiments. Xenograft studies in severe combined immunodeficient (SCID) mice with PANC-1, HPAF-II and BxPC3 cell lines were performed with $2x10^5$ cells resuspended in serum-free medium and injected subcutaneously in the abdominal cavity of the mice. The mice were kept for up to 3 months and tumor measurements were taken bi-weekly. When tumors reached a diameter of 1.5 cm or became ulcerated, the mice were sacrificed by carbon dioxide asphyxiation. The tumors were removed, weighed, measured and fixed in 10% buffered formalin for histologic processing or flash-frozen in liquid nitrogen for protein and/or RNA analysis. 5 injections were performed per condition and each cell line was performed in duplicate. Tumor measurements were taken with a calliper

and tumor volume was calculated by the ellipsoid formula $V = \pi/6 \times (l \times w^2)$, where l and w denote the longest and shortest tumor axis, respectively.

Supplemental References

Bakal, C.J., Finan, D., LaRose, J., Wells, C.D., Gish, G., Kulkarni, S., DeSepulveda, P., Wilde, A. and Rottapel, R. (2005). The Rho GTP exchange factor Lfc promotes spindle assembly in early mitosis. Proc. Natl. Acad. Sci. U. S. A. *27,* 9529-9534.

Balin-Gauthier, D., Delord, J.P., Rochaix, P., Mallard, V., Thomas, F., Hennebelle, I., Bugat, R., Canal, P., and Allal, C. (2006). In vivo and in vitro antitumor activity of oxaliplatin in combination with cetuximab in human colorectal tumor cell lines expressing different level of EGFR. Cancer Chemother. Pharmacol. *57*, 709-718.

Davies, B.R., Greenwood, H., Dudley, P., Crafter, C., Yu, D.H., Zhang, J., Li, J., Gao, B., Ji, Q., Maynard, J. *et al*. (2012). Preclinical pharmacology of AZD5363, an inhibitor of AKT: pharmacodynamics, antitumor activity, and correlation of monotherapy activity with genetic background. Mol. Cancer Ther. *11*, 873-887.

Hoeflich, K.P., O'Brien, C., Boyd, Z., Cavet, G., Guerrero, S., Jung, K., Januario, T., Savage, H., Punnoose, E., Truong, T., *et al*. (2009). In vivo antitumor activity of MEK and phosphatidylinositol 3-kinase inhibitors in basal-like breast cancer models. Clin. Cancer Res. *15*, 4649-4664.

Holford, J., Rogers, P., and Kelland, L.R. (1998). Ras mutation and platinum resistance in human ovarian carcinomas in vitro. Int. J. Cancer *77*, 94-100.

Hollestelle, A., Elstrodt, F., Nagel, J.H.A., Kallemeijn, W.W., Schutte, M. (2007). Phosphatidylinositol-3-OH kinase or RAS pathway mutations in human breast cancer cell lines. Mol. Cancer Res. *5*, 195-201.

Ikediobi, O.N., Davies, H., Bignell, G., Edkins, S., Stevens, C., O'Meara, S., Santarius, T., Avis, T., Barthorpe, S., Brackenbury, L., *et al*. (2006). Mutation analysis of 24 known cancer genes in the NCI-60 cell line set. Mol. Cancer Ther. *5*, 2606-2612.

Kozma, S.C., Bogaard, M.E., Buser, K., Saurer, S.M., Bos, J.L., Groner, B., and Hynes, N.E. (1987). The human c-Kirsten ras gene is activated by a novel mutation in codon 13 in the breast carcinoma cell line MDA-MB231. Nucleic Acids Res. *15*, 5963–5971.

Kraus, M.H., Yuasa, Y., and Aaronson, S.A. (1984). A position 12-activated H- ras oncogene in all HS578T mammary carcinosarcoma cells but not normal mammary cells of the same patient. Proc. Natl. Acad. Sci. U.S.A. *81*, 5384–5388.

Letourneau, I.J., Quinn, M.C.J., Wang, L., Portelance, L., Caceres, K.Y., Cyr, L., Delvoye, N., Meunier, L., De Ladurantaye, M., Shen, Z., *et al*. (2012). Derivation and characterization of matched cell lines from primary and recurrent serous ovarian cancer. B.M.C. Cancer *12*, 379-395.

Marshall, C.B., Meiri, D., Smith, M.J., Mazhab-Jafari, M.T., Gasmi-Seabrook, G.M., Rottapel, R., Stambolic, V. and Ikura, M. (2012). Probing the GTPase cycle with real-time NMR: GAP and GEF activities in cell extracts. Methods *4,* 473-485.

Muller, J., Ory, S., Copeland, T., Piwnica-Worms, H. and Morrison, D.K. (2001). C-TAK1 regulates Ras signaling by phosphorylating the MAPK scaffold, KSR1. Mol. Cell *5,* 983-993.

Ouellet,, V., Zietarska, M., Portelance, L., Lafontaine, J., Madore, J., Puiffe, M.L., Arcand, S.L., Shen, Z., Hebert, J., Tonin, P.N., *et al*. (2008). Characterization of three new serous epithelial ovarian cancer cell lines. B.M.C. Cancer *8*, 152-169.

Patton, S.E., Martin, M.L., Nelsen, L.L., Fang, X., Mills, G.B., Bast, R.C. Jr., and Ostrowski, M.C. (1998). Activation of the ras-mitogen-activated protein kinase pathway and

phosphorylation of ets-2 at position threonine 72 in human ovarian cancer cell lines. Cancer Res. *58*, 2253-2259.